



1 Anthropogenic Secondary Organic Aerosols Contribute Substantially to Air Pollution 2 Mortality

3
4 Benjamin A. Nault^{1,2,*}, Duseong S. Jo^{1,2}, Brian C. McDonald^{2,3}, Pedro Campuzano-Jost^{1,2}, Douglas A.
5 Day^{1,2}, Weiwei Hu^{1,2,**}, Jason C. Schroder^{1,2,***}, James Allan^{4,5}, Donald R. Blake⁶, Manjula R.
6 Canagaratna⁷, Hugh Coe⁵, Matthew M. Coggon^{2,3}, Peter F. DeCarlo⁸, Glenn S. Diskin⁹, Rachel
7 Dunmore¹⁰, Frank Flocke¹¹, Alan Fried¹², Jessica B. Gilman³, Georgios Gkatzelis^{2,3}, Jacqui F. Hamilton¹⁰,
8 Thomas F. Hanisco¹³, Patrick L. Hayes¹⁴, Daven K. Henze¹⁵, Alma Hodzic^{11,16}, James Hopkins^{10,17}, Min
9 Hu¹⁸, L. Gregory Huey¹⁹, B. Thomas Jobson²⁰, William C. Kuster^{3,****}, Alastair Lewis^{10,17}, Meng Li^{2,3}, Jin
10 Liao^{13,21}, M. Omar Nawaz¹⁵, Ilana B. Pollack²², Jeffrey Peischl^{2,3}, Bernhard Rappenglück²³, Claire E.
11 Reeves²⁴, Dirk Richter¹², James M. Roberts³, Thomas B. Ryerson³, Min Shao²⁵, Jacob M. Sommers^{14,26},
12 James Walega¹², Carsten Warneke^{2,3}, Petter Weibring¹², Glenn M. Wolfe^{13,27}, Dominique E. Young^{5,*****},
13 Bin Yuan²⁵, Qiang Zhang²⁸, Joost A. de Gouw^{1,2}, and Jose L. Jimenez^{1,2,+}

- 14
15 1. Department of Chemistry, University of Colorado, Boulder, Boulder, CO, USA
16 2. Cooperative Institute for Research in Environmental Sciences, Boulder, Colorado, USA
17 3. Chemical Sciences Division, NOAA Earth System Research Laboratory, Boulder, CO
18 4. National Centre for Atmospheric Sciences, School of Earth and Environmental Sciences, University of Manchester, Manchester, UK
19 5. Centre of Atmospheric Science, School of Earth and Environmental Sciences, University of Manchester, Manchester, UK
20 6. Department of Chemistry, University of California, Irvine, Irvine, CA, USA
21 7. Center for Aerosol and Cloud Chemistry, Aerodyne Research Inc., Billerica, MA, USA
22 8. Department of Environmental Health Engineering, Johns Hopkins University, Baltimore, MD, USA
23 9. NASA Langley Research Center, Hampton, Virginia, USA
24 10. Wolfson Atmospheric Chemistry Laboratories, Department of Chemistry, University of York, York, UK
25 11. Atmospheric Chemistry Observations and Modeling Laboratory, National Center for Atmospheric Research, Boulder, CO, USA
26 12. Institute of Arctic and Alpine Research, University of Colorado, Boulder, CO, USA
27 13. Atmospheric Chemistry and Dynamic Laboratory, NASA Goddard Space Flight Center, Greenbelt, MD, USA
28 14. Department of Chemistry, Université de Montréal, Montréal, QC, Canada
29 15. Department of Mechanical Engineering, University of Colorado, Boulder, Boulder, CO, USA
30 16. Laboratoires d'Aréologie, Université de Toulouse, CNRS, UPS, Toulouse, France
31 17. National Centre for Atmospheric Sciences, Department of Chemistry, University of York, York, UK
32 18. State Key Joint Laboratory of Environmental Simulation and Pollution Control, College of Environmental Sciences and Engineering, Peking
33 University, Beijing, China
34 19. School of Earth and Atmospheric Sciences, Georgia Institute of Technology, Atlanta, Georgia, USA
35 20. Laboratory for Atmospheric Research, Department of Civil and Environmental Engineering, Washington State University, Pullman, WA,
36 USA
37 21. Universities Space Research Association, GESTAR, Columbia, MD, USA
38 22. Department of Atmospheric Science, Colorado State University, Fort Collins, CO, USA
39 23. Department of Earth and Atmospheric Science, University of Houston, Houston, TX, USA
40 24. Centre for Ocean and Atmospheric Sciences, School of Environmental Sciences, University of East Anglia, Norwich, UK
41 25. Institute for Environmental and Climate Research, Jinan University, Guangzhou, China
42 26. Air Quality Research Division, Environment and Climate Change Canada, Toronto, Ontario, Canada
43 27. Joint Center for Earth Systems Technology, University of Maryland, Baltimore County, Baltimore, MD, USA
44 28. Ministry of Education Key Laboratory for Earth System Modeling, Department of Earth System Science, Tsinghua University, Beijing, China
45 *Now at Center for Aerosol and Cloud Chemistry, Aerodyne Research Inc., Billerica, MA, USA
46 **Now at State Key Laboratory at Organic Geochemistry, Guangzhou Institute of Geochemistry, Chinese Academy of Sciences, Guangzhou,
47 China
48 ***Now at Colorado Department of Public Health and Environment, Denver, CO, USA
49 ****Has retired and worked on this manuscript as an unaffiliated co-author.
50 *****Now at Air Quality Research Center, University of California, Davis, CA, USA
51
52 +Corresponding author: Jose L. Jimenez (jose.jimenez@colorado.edu)



53 **Abstract**

54 Anthropogenic secondary organic aerosol (ASOA), formed from anthropogenic emissions of
55 organic compounds, constitutes a substantial fraction of the mass of submicron aerosol in
56 populated areas around the world and contributes to poor air quality and premature mortality.
57 However, the precursor sources of ASOA are poorly understood, and there are large uncertainties
58 in the health benefits that might accrue from reducing anthropogenic organic emissions. We
59 show that the production of ASOA in 11 urban areas on three continents is strongly correlated
60 with the anthropogenic reactivity of specific volatile organic compounds. The differences in
61 ASOA production across different cities can be explained by differences in the emissions of
62 aromatics and intermediate- and semi-volatile organic compounds, indicating the importance of
63 controlling these ASOA precursors. With an improved modeling representation of ASOA driven
64 by the observations, we attribute 340,000 $PM_{2.5}$ premature deaths per year to ASOA, which is
65 over an order of magnitude higher than prior studies. A sensitivity case with a more recently
66 proposed model for attributing mortality to $PM_{2.5}$ (the Global Exposure Mortality Model) results
67 up to 900,000 deaths. A limitation of this study is the extrapolation from regions with detailed
68 data to others where data is not available. Comprehensive air quality campaigns in the countries
69 in South and Central America, Africa, South Asia, and the Middle East are needed for further
70 progress in this area.



71 **1. Introduction**

72 Poor air quality is one of the leading causes of premature mortality worldwide (Cohen et
73 al., 2017; Landrigan et al., 2018). Roughly 95% of the world's population live in areas where
74 $PM_{2.5}$ (fine particulate matter with diameter smaller than $2.5 \mu m$) exceeds the World Health
75 Organization's $10 \mu g m^{-3}$ annual average guideline (Shaddick et al., 2018). This is especially true
76 for urban areas, where high population density is co-located with increased emissions of $PM_{2.5}$
77 and its gas-phase precursors from human activities. It is estimated that $PM_{2.5}$ leads to 3 to 4
78 million premature deaths per year, higher than the deaths associated with other air pollutants
79 (Cohen et al., 2017). More recent analysis using concentration-response relationships derived
80 from studies of populations exposure to high levels of ambient $PM_{2.5}$ suggest the global
81 premature death burden could be up to twice this value (Burnett et al., 2018).

82 The average measured chemical composition of submicron PM (PM_1 , which typically
83 comprises most of $PM_{2.5}$ (Wang et al., 2015)) for various megacities, urban areas, and outflow
84 regions around the world is shown in Fig. 1. A substantial fraction of urban PM_1 is organic
85 aerosol (OA), which is composed of primary OA (POA, organic compounds emitted directly in
86 the particle phase) and secondary OA (SOA, formed from chemical reactions of precursor
87 organic gases). SOA is typically a factor of 2 to 3 higher than POA for these locations.

88 Understanding the gas-phase precursors of anthropogenic SOA (ASOA, defined as the
89 SOA formed from anthropogenic volatile organic compounds (AVOC) (de Gouw et al., 2005;
90 DeCarlo et al., 2010)) quantitatively is challenging (Hallquist et al., 2009). Though the
91 enhancement of ASOA is largest in large cities, these precursors and production of ASOA should
92 be important in any location impacted by anthropogenic emissions (e.g., Fig. 1). ASOA



93 comprises a wide range of condensable products generated by numerous chemical reactions
94 involving AVOC precursors (Hallquist et al., 2009; Hayes et al., 2015; Shrivastava et al., 2017).
95 These condensable products include intermediate volatile organic compounds (IVOCs, less
96 volatile than traditional VOCs and often not measured or considered (Robinson et al., 2007;
97 Hayes et al., 2015)) and semi volatile organic compounds (SVOCs, less volatile than IVOC and
98 similarly not measured or considered).

99 The main categories of gas-phase precursors that dominate ASOA have been the subject
100 of intensive research. Transportation-related emissions (e.g., tailpipe, evaporation, refueling)
101 were assumed to be the major precursors of ASOA, which was supported by field studies
102 (Parrish et al., 2009; Gentner et al., 2012; Warneke et al., 2012; Pollack et al., 2013). Yet, budget
103 closure of observed ASOA mass concentrations could not be achieved with
104 transportation-related VOCs (Ensberg et al., 2014). The contribution of urban-emitted biogenic
105 precursors to SOA in urban areas is typically small, and rather, the contribution of biogenic SOA
106 (BSOA) in urban areas is typically dominated by regionally advected SOA background (e.g.,
107 Hodzic et al., 2009, 2010a; Hayes et al., 2013; Janssen et al., 2017). BSOA is thought to
108 dominate globally (Hallquist et al., 2009), but as shown in Fig. 1, the contribution of BSOA (1%
109 to 20%) to urban concentrations, while often substantial, is typically smaller than that of ASOA
110 (17% to 39%) (see Sect. 2). Recent studies have indicated that emissions from volatile chemical
111 products (VCPs), defined as pesticides, coatings, inks, adhesives, personal care products, and
112 cleaning agents (McDonald et al., 2018), as well as cooking emissions (Hayes et al., 2015), are
113 important. While total amounts of ASOA precursors released in cities have dramatically declined
114 (largely due to three-way catalytic converters in cars (Warneke et al., 2012; Pollack et al., 2013;



115 Zhao et al., 2017; Khare and Gentner, 2018)), VCPs have not declined as quickly (Khare and
116 Gentner, 2018; McDonald et al., 2018). Besides a few cities in the US (Coggon et al., 2018;
117 Khare and Gentner, 2018; McDonald et al., 2018), extensive VCP emission quantification has
118 not yet been published.

119 Due to the uncertainty on the ASOA precursors and on the amount of ASOA formed
120 from them, the number of premature deaths associated with urban organic emissions is largely
121 unknown. Currently, most studies have not included ASOA realistically (e.g., Lelieveld et al.,
122 2015; Silva et al., 2016; Ridley et al., 2018) in source apportionment calculations of the
123 premature deaths associated with long-term exposure of $PM_{2.5}$. These models represented total
124 OA as non-volatile POA and “traditional” ASOA precursors (transportation-based VOCs), which
125 largely under-predict ASOA (Ensberg et al., 2014; Hayes et al., 2015; Nault et al., 2018;
126 Schroder et al., 2018) given that the current understanding is that POA is volatile and contributes
127 to ASOA mass concentration (e.g., Grieshop et al., 2009; Lu et al., 2018). As PM_1 and SOA
128 mass are highest in urban areas (Fig. 1), also shown in Jimenez et al. (2009), it is necessary to
129 quantify the amount and identify the sources of ASOA to target future emission standards that
130 will optimally improve air quality and the associated health impacts. As these emissions are from
131 human activities, they will contribute to SOA mass outside urban regions and to potential health
132 impacts outside urban regions as well.

133 Here, we investigate the factors that control ASOA using 11 major urban, including
134 megacities, field studies (Fig. 1 and Table 1). The empirical relationships and numerical models
135 are then used to quantify the attribution of premature mortality to ASOA around the world, using
136 the observations to improve the modeled representation of ASOA. The results provide insight



137 into the importance of ASOA to global premature mortality due to $PM_{2.5}$ and further
138 understanding the precursors and sources of ASOA in urban regions.

139

140 **2. Methods**

141 **2.1 Ambient Observations**

142 For values not previously reported in the literature (Table S4), observations taken
143 between 11:00 – 16:00 local time were used to determine the slopes of SOA versus
144 formaldehyde (HCHO) (Fig. S2), peroxy acetyl nitrate (PAN) (Fig. S3), and O_x ($O_x = O_3 + NO_2$)
145 (Fig. S4). For CalNex, there was an approximate 48% difference between the two HCHO
146 measurements (Fig. S1). Therefore, the average between the two measurements were used in this
147 study, similar to what has been done in other studies for other gas-phase species (Bertram et al.,
148 2007). All linear fits, unless otherwise noted, use the orthogonal distance regression fitting
149 method (ODR).

150 For values in Table S4 through Table S8 not previously reported in the literature, the
151 following procedure was applied to determine the emissions ratios, similar to the methods of
152 Nault et al. (2018). An OH exposure ($OH_{exp} = [OH] \times \Delta t$), which is also the photochemical age
153 (PA), was estimated by using the ratio of NO_x/NO_y (Eq. 1) or the ratio of
154 m+p-xylene/ethylbenzene (Eq. 2). For the m+p-xylene/ethylbenzene, the emission ratio
155 (Table S5) was determined by determining the average ratio during minimal photochemistry,
156 similar to prior studies (de Gouw et al., 2017). This was done for only one study, TexAQS 2000.
157 This method could be applied in that case as it was a ground campaign that operated both day
158 and night; therefore, a ratio at night could be determined when there was minimal loss of both



159 VOCs. The average emission ratio for the other VOCs was determined using Eq. 3 after the
160 OH_{exp} was calculated in Eq. 1 or Eq. 2. The rate constants used for determining OH_{exp} and
161 emission ratios are found in Table S11.

$$162 \quad OH_{exp} = [OH] \times t = \ln \left(\frac{\left(\frac{[NO_x]}{[NO_y]} \right)}{k_{OH+NO_2}} \right) \quad \text{Eq. 1}$$

$$163 \quad OH_{exp} = [OH] \times t = - \frac{1}{k_{m+p-xylene} - k_{ethylbenzene}} \times \ln \left(\frac{[m+p-xylene]_t}{[ethylbenzene]_t} - \frac{[m+p-xylene]_0}{[ethylbenzene]_0} \right) \quad \text{Eq. 2}$$

$$164 \quad \frac{[VOC(i)]}{[CO]}(0) = - \frac{[VOC(i)]}{[CO]}(t) \times \left(1 - \frac{1}{\exp(-k_i \times [OH] \times t)} \right) \times k_i + \frac{[VOC(i)]}{[CO]}(t) \times k_i \quad \text{Eq. 3}$$

167

168 2.2 Error Analysis of Observations

169 The errors that will be discussed here are in reference to Fig. 5 and Fig. 6 and Table S4
170 either come from the 1σ uncertainty in the slopes (the SOA versus O_x , HCHO, or PAN values) or
171 propagation of uncertainty in observations. For SOA, we estimate the 1σ uncertainty of ~15%,
172 which is lower than the typical 1σ uncertainty of the AMS (Bahreini et al., 2009) due to the
173 careful calibrations and excellent intercomparisons in the various campaigns (see Table 1 for
174 references for the AMS comparisons). For ΔCO , the largest uncertainty is associated with the
175 CO background (Hayes et al., 2013; Nault et al., 2018), and is estimated to be ~10% at 0.5
176 photochemical equivalent days (Hayes et al., 2013). The uncertainty in the emission ratios is
177 ~10% (Wang et al., 2014; de Gouw et al., 2017); though, it may be higher for the values



178 calculated here (see above) due to the uncertainty in CO background, rate constants, and
179 photochemical age. Therefore, for Fig. 5a, the uncertainty in the y-values is 18% and the
180 uncertainty in the x-values is 10%. For Fig. 6, the uncertainty in the measurement is 21%.

181 Another potential source of uncertainty may stem from the fit of the data in Fig. 5a, as the
182 data point from Seoul (KORUS-AQ) could be impacting the fit due to the difference in its value
183 compared to the other locations. A sensitivity analysis, where one study was removed and a new
184 fit was derived, was conducted to determine the impact of any one study on the fit reported in
185 Fig. 5a (see Table S10). We find that though removing the Seoul data point increases the slope,
186 the value is still within the uncertainty and statistically significant at the 95% confidence
187 interval. Thus, the data from Seoul does not change the results and conclusions reported in this
188 study.

189

190 **2.3 Emission Inventories for Various Urban Areas around the World**

191 All BTEX (benzene, toluene, ethylbenzene, and xylenes) and non-BTEX aromatic emissions
192 are shown in Table S5 (BTEX) or Table S8 (non-BTEX aromatics) and are described above. The
193 emission ratios are derived from ambient measurements utilizing photochemical aging
194 techniques (Nault et al., 2018).

195 Details of the emission inventories for cities in the US, for Beijing, and for London/UK
196 used here to estimate the IVOC:BTEX emission ratio (Fig. 2) and thus the IVOC emissions can
197 be found in SI Sect. 1 through 3. Briefly, emissions for the US are based on McDonald et al.
198 (2018), for China on the Multi-resolution Emission Inventory for China (MEIC) (Zhang et al.,
199 2009; Zheng et al., 2014, 2018; Liu et al., 2015; Li et al., 2017, 2019), and for the UK on the



200 National Atmospheric Emissions Inventory (NAEI) (EMEP/EEA, 2016). The IVOC:BTEX
201 emission ratio from inventories are multiplied with the observed BTEX measured in urban air to
202 estimate IVOCs emitted in each region (Table S5), including North America, Europe, and Asia.
203 This ensures IVOC emissions used in our calculations properly reflect differences in mixtures of
204 emission sources (e.g., mobile sources versus VCPs) that vary by continent for each field
205 campaign. Additionally, we rely on inventories for estimating atmospheric abundances of IVOCs
206 because it has been challenging to measure the full range of IVOC precursors that are emitted
207 into urban air (Zhao et al., 2014, 2017; Lu et al., 2018). In particular, many of the IVOCs emitted
208 from VCPs are oxygenated, which are challenging to measure using traditional gas
209 chromatography-mass spectrometry (GC-MS) techniques. Oxygenated IVOCs may not elute
210 completely through a non-polar column, and are likely underestimated (Zhao et al., 2014). The
211 bottom-up IVOC:BTEX ratios for the US, Beijing, and UK are described in greater detail in SI
212 Sect. S1 through S3. IVOC emissions are classified based on their vapor pressure (effective
213 saturation concentration: $0.3 < C^* < 3 \times 10^6 \mu\text{g m}^{-3}$), with the vapor pressure estimated by the
214 SIMPOL.1 model (Pankow and Asher, 2008). Unspeciated mass has been suggested as important
215 SOA precursors from gasoline and diesel engines, and parameterized by n-tridecane and
216 n-pentadecane, respectively (Jathar et al., 2014). For VCPs, the volatility distribution of VOCs is
217 in-between that of gasoline and diesel fuel. Therefore, n-tetradecane was suggested as a
218 surrogate for unspeciated mass of VCPs by McDonald et al. (2018).

219 Similar to IVOCs, the ability to measure the full range of SVOCs emitted into urban air is
220 challenging. Therefore, we estimate SVOC emission ratios relative to POA mass concentrations
221 (Table S9), as described by Ma et al. (2017). For the hydrocarbon-like portion, we used the



222 volatility distribution from Worton et al. (2014) to estimate SVOC, as this is associated with
223 fossil fuel emissions from transportation (Zhang et al., 2005). For the other POA, we used the
224 volatility distribution from Robinson et al. (2007), as this POA is typically cooking primary
225 aerosol.

226 Fig. 3 shows the calculated emission ratio versus saturation concentration (c^*) for the
227 cities with emission inventories. The saturation concentration for SVOC was determined as part
228 of the estimation procedure discussed above. For IVOC, the emission ratios for the different
229 sources (gasoline, diesel, other fossil fuel sources, and VCP emissions) were split into the
230 volatility bins, as in McDonald et al. (2018). Finally, for BTEX and non-BTEX aromatics, and
231 other VOC emission ratios (see Fig. 3 for references for the other VOC emission ratios), CRC
232 (Rumble, 2019) or SIMPOL.1 (Pankow and Asher, 2008) (for estimating vapor pressures not in
233 CRC) was used to estimate the saturation concentrations.

234

235 **2.4 ASOA Budget Analysis of Ambient Observations**

236 To calculate the ASOA budget, we used the observed BTEX (Table S5) and non-BTEX
237 aromatic (Table S8) emission ratios, the emission inventories for IVOC (see above), and
238 estimated SVOCs from the primary OA emissions (see above). The methods to calculate ASOA
239 from emissions have been described in detail elsewhere (Hayes et al., 2015; Ma et al., 2017;
240 Schroder et al., 2018), and are briefly described here. All calculations described were conducted
241 with the KinSim v4.02 chemical kinetics simulator (Peng and Jimenez, 2019) within Igor Pro 7
242 (Lake Oswego, Oregon), and are summarized in Fig. S5. A typical average particle diameter for
243 urban environments of ~ 200 nm (Seinfeld and Pandis, 2006) is used to estimate the



244 condensational sink term for the partitioning of gas-to-particle, although condensation is always
245 fast compared to the experiment timescales. Further, we assume an average 250 g mol^{-1} molar
246 mass for OA and an average SOA density of 1.4 g cm^{-3} (Vaden et al., 2011; Kuwata et al., 2012).
247 Finally, all models are initialized with the campaign specific OA background (typically $\sim 2 \mu\text{g}$
248 sm^{-3}) and POA (Table S9) for partitioning of gases to the particle phase, and ran at the average
249 temperature for the campaign.

250 For the modeled VOCs (BTEX and non-BTEX aromatics), each species undergoes
251 temperature-dependent OH oxidation (Table S11), forming four SVOCs that partition between
252 gas- and particle-phase, using updated SOA yields that account for wall loss (Ma et al., 2017).
253 For IVOCs, the emission weighted SOA yields and rate constants from the “Zhao” option (Zhao
254 et al., 2014) of Ma et al. (2017) are used, and the products are apportioned into three SVOC bins
255 and one low-volatility organic compound (LVOC) bin (Fig. S5). Finally, SVOCs undergo
256 photooxidation at a rate of $4 \times 10^{-11} \text{ cm}^3 \text{ molecules}^{-1} \text{ s}^{-1}$ (Dzepina et al., 2009; Hodzic et al.,
257 2010b; Tsimpidi et al., 2010; Hodzic and Jimenez, 2011; Hayes et al., 2015; Ma et al., 2017;
258 Schroder et al., 2018), producing one product per oxidation step, with yields from Robinson et al.
259 (2007) for cooking and other SVOCs and yields from Worton et al. (2014) for fossil fuel related
260 SVOCs, as recommended by Ma et al. (2017). The products from SVOC and IVOC oxidation are
261 allowed to further oxidize, as highlighted in Fig. S5 and described in prior studies (Hayes et al.,
262 2015; Ma et al., 2017; Schroder et al., 2018). Generally, each product reacts at a rate of 4×10^{-11}
263 $\text{cm}^3 \text{ molecules}^{-1} \text{ s}^{-1}$ to produce some product at one volatility bin lower, adding one oxygen to the
264 compound for each oxidation (Dzepina et al., 2009; Tsimpidi et al., 2010; Hodzic and Jimenez,
265 2011; Hayes et al., 2015; Ma et al., 2017; Schroder et al., 2018). An update includes



266 fragmentation for a fraction of the molecules that are oxidized, as described in Schroder et al.
267 (2018) and Koo et al. (2014). As shown in Fig. S5, fragmentation of the compound occurs as it is
268 oxidized and goes down one volatility bin. For further oxidation of SVOCs from the oxidation of
269 primary IVOCs, one oxygen is added and 0.25 carbon is removed per step, leading to an increase
270 in mass of 1.03 (instead of 1.07) per oxidation step (Koo et al., 2014; Schroder et al., 2018). For
271 further oxidation of products from primary SVOC emissions, one oxygen is added and 0.5
272 carbon is removed per step, leading to an increase in mass of 0.99 (instead of 1.07) per oxidation
273 step (Koo et al., 2014; Nault et al., 2018).

274

275 **2.5 GEOS-Chem Modeling**

276 The model used in this study, for ASOA apportionment (Fig. 1), for apportionment of
277 ASOA to total PM_{2.5} for premature mortality calculations (Worldwide Premature Deaths Due to
278 ASOA), and for sensitivity analysis for ASOA production and emissions on premature mortality
279 calculations, is the GEOS-Chem v12.0.0 global chemical transport model (Bey et al., 2001; The
280 International GEOS-Chem User Community, 2018) to calculate global concentrations of PM_{2.5}
281 and ASOA at 2°×2.5° horizontal resolution. Goddard Earth Observing System – Forward
282 Processing (GEOS-FP) assimilated data from the NASA Global Modeling and Assimilation
283 Office (GMAO) were used for input meteorological fields. The model was run for 2013 to 2018
284 to take into account interannual variability of meteorological impacts onto PM_{2.5} (therefore,
285 averaging PM_{2.5} over variations in meteorology). However, the HTAPv2 emission inventory,
286 which was used for anthropogenic emissions (Janssens-Maenhout et al., 2015), was kept constant
287 for the 5 years. GEOS-Chem simulates gas and aerosol chemistry with ~700 chemical reactions.



288 GEOS-Chem calculates the following $PM_{2.5}$ species: sulfate, ammonium, nitrate (Park et al.,
289 2006); black carbon and POA (Park et al., 2005); SOA (Pye and Seinfeld, 2010; Marais et al.,
290 2016); sea salt (accumulation mode only (Jaeglé et al., 2011)); and, dust (Duncan Fairlie et al.,
291 2007).

292

293 **2.5.1 Biogenic SOA**

294 For monoterpene and sesquiterpene SOAs, we used the default complex SOA scheme
295 (without semi-volatile POA) using the two-product model framework (Pye and Seinfeld, 2010).
296 This scheme calculates initial oxidation of VOCs with OH, O_3 , and NO_3 , and resulting products
297 are assigned to four different gas-phase semi-volatile species (TSOA0–3) based on volatilities
298 ($c^* = 0.1, 1, 10, 100 \mu g m^{-3}$). Aerosol and gas species fractions are calculated online using the
299 partitioning theory, and all are removed by dry and wet deposition processes.

300 For isoprene SOA, we used the explicit isoprene chemistry developed by Marais et al.
301 (2016). All the isoprene-derived gas-phase products, including isoprene peroxy radical,
302 ISOPOOH, IEPOX, glyoxal, and methylglyoxal, are explicitly simulated. Irreversible
303 heterogeneous uptake of precursors to aqueous aerosols are further calculated using online
304 aerosol pH and surface area.

305 GEOS-Chem was used to estimate the relative fractions of the measured SOA in our
306 studies between anthropogenic and biogenic (isoprene and monoterpene) sources (Fig. 1).
307 Extensive research has been conducted to evaluate and improve the models performance in
308 predicting BSOA, as summarized in Table S3. Though these evaluations mainly occurred in the
309 southeast US, a recent study has also included more global observations to compare with



310 GEOS-Chem (Pai et al., 2020). Generally, GEOS-Chem appears to overestimate biogenically
311 derived SOA; however, the model predicted SOA is typically within the uncertainty of the AMS
312 (Table S3). The overestimation, though, would suggest that the fraction of urban SOA may be
313 under-predicted by this method, whereas the BSOA may be over-predicted. Therefore, in urban
314 regions, the amount of SOA from biogenic sources may be lower, especially after the rapid SOA
315 enhancements (within 12 to 24 equivalent photochemical hours that have been observed around
316 the world (Nault et al., 2018)). Typically the BSOA is present as a regional background and
317 subtracted for the analyses used in this work, which focus on strong urban plumes on top of that
318 background (Hayes et al., 2013, 2015).

319

320 **2.5.2 Default GEOS-Chem Sensitivity to ASOA Simulations**

321 For the sensitivity calculation using the "traditional" ASOA precursors, we used the
322 two-product model framework (Pye and Seinfeld, 2010). Benzene, toluene, and xylene are
323 oxidized with OH and converted to peroxy radicals. These peroxy radicals react with HO₂ or NO,
324 resulting in non-volatile ASOA (HO₂ pathway, ASOAN species in GEOS-Chem) or
325 semi-volatile ASOA tracers (NO pathway, ASOA1-3 in GEOS-Chem). As is the case for
326 monoterpene and sesquiterpene SOA above, GEOS-Chem calculates online partitioning and
327 dry/wet deposition processes for semi-volatile ASOA tracers. Other conditions including
328 mortality calculation are kept the same as the base simulation above.

329

330 **2.6 Estimation of Premature Mortality Attribution**



331 Premature deaths were calculated for five disease categories: ischemic heart disease
332 (IHD), stroke, chronic obstructive pulmonary disease (COPD), acute lower respiratory illness
333 (ALRI), and lung cancer (LC). We calculated premature mortality for the population aged more
334 than 30 years, using Eq. 4.

$$335 \quad \text{Premature Death} = \text{Pop} \times y_0 \times \frac{RR - 1}{RR} \quad \text{Eq. 4}$$

336 Mortality rate, y_0 , varies according to the particular disease category and geographic region,
337 which is available from Global Burden of Disease (GBD) Study 2015 database (IHME, 2016).
338 Population (Pop) was obtained from Columbia University Center for International Earth Science
339 Information Network (CIESIN) for 2010 (CIESIN, 2017). Relative risk, RR, can be calculated as
340 shown in Eq. 5.

$$341 \quad RR = 1 + \alpha \times \left(1 - \exp\left(\beta \times (PM_{2.5} - PM_{2.5,Threshold})^\rho\right) \right) \quad \text{Eq. 5}$$

342 α , β , and ρ values depend on disease category and are calculated from Burnett et al. (2014) (see
343 Table S12 and associated file). If the $PM_{2.5}$ concentrations are below the $PM_{2.5}$ threshold value
344 (Table S12), premature deaths were computed as zero. However, there could be some health
345 impacts at concentrations below the $PM_{2.5}$ threshold values (Krewski et al., 2009); following the
346 methods of the GBD studies, these can be viewed as lower bounds on estimates of premature
347 deaths.

348 We performed an additional sensitivity analysis using the Global Exposure Mortality
349 Model (GEMM) (Burnett et al., 2018). For the GEMM analysis, we also used age stratified
350 population data from GWPv3. Premature death is calculated the same as shown in Eq. 4;
351 however, the relative risk differs. For the GEMM model, the relative risk can be calculated as
352 shown in Eq. 6.



$$RR = \exp(\theta \times \lambda) \text{ with } \lambda = \frac{\log\left(1 + \frac{z}{\alpha}\right)}{\left(1 + \exp\left(\frac{(\hat{\mu} - z)}{\pi}\right)\right)}$$

Eq. 6

Here $z = \max(0, PM_{2.5} - PM_{2.5, \text{Threshold}})$; θ , π , $\hat{\mu}$, α , and $PM_{2.5, \text{Threshold}}$ depends on disease category and are from Burnett et al. (2018). Similar to the Eq. 5, if the concentrations are below the threshold ($2.4 \mu\text{g m}^{-3}$, Burnett et al. (2018)), then premature deaths are computed as zero; however, the GEMM has a lower threshold than the GBD method.

For GBD, we do not consider age-specific mortality rates or risks. For GEMM, we calculate age-specific health impacts with age-specific parameters in the exposure response function (Table S13). We combine the age-specific results of the exposure-response function with age distributed population data from GPW (CIESIN, 2017) and a national mortality rate across all ages to assess age-specific mortality.

We calculated total premature deaths using annual average total $PM_{2.5}$ concentrations derived from satellite-based estimates at the resolution of $0.1^\circ \times 0.1^\circ$ from van Donkelaar et al. (2016). Application of the remote-sensing based $PM_{2.5}$ at the $0.1^\circ \times 0.1^\circ$ resolution rather than direct use of the GEOS-Chem model concentrations at the $2^\circ \times 2.5^\circ$ resolution helps reduce uncertainties in the quantification of $PM_{2.5}$ exposure inherent in coarser estimates (Punger and West, 2013). We also calculated deaths by subtracting from this amount the total annual average ASOA concentrations derived from GEOS-Chem (Fig. S9). To reduce uncertainties related to spatial gradients and total concentration magnitudes in our GEOS-Chem simulations of $PM_{2.5}$, our modeled ASOA was calculated as the fraction of ASOA to total $PM_{2.5}$ in GEOS-Chem, multiplied by the satellite-based $PM_{2.5}$ concentrations (Eq. 7).

$$ASOA_{\text{sat}} = (ASOA_{\text{mod}} / PM_{2.5, \text{mod}}) \times PM_{2.5, \text{sat}}$$

Eq. 7



374 Finally, this process for estimating $PM_{2.5}$ health impacts considers only $PM_{2.5}$ mass concentration
375 and does not distinguish toxicity by composition, consistent with the current US EPA position
376 expressed in Sacks et al. (2019).

377

378 **3. Observations of ASOA Production across Three Continents**

379 **3.1 Observational Constraints of ASOA Production across Three Continents**

380 Measurements during intensive field campaigns in large urban areas better constrain
381 concentrations and atmospheric formation of ASOA because the scale of ASOA enhancement is
382 large compared to SOA from regional background. Generally, ASOA increased with the amount
383 of urban precursor VOCs and with atmospheric PA (de Gouw et al., 2005; de Gouw and Jimenez,
384 2009; DeCarlo et al., 2010; Hayes et al., 2013; Nault et al., 2018; Schroder et al., 2018; Shah et
385 al., 2018). In addition, ASOA correlates strongly with gas-phase secondary photochemical
386 species, including O_x , HCHO, and PAN (Herndon et al., 2008; Wood et al., 2010; Hayes et al.,
387 2013; Zhang et al., 2015; Nault et al., 2018; Liao et al., 2019) (Table S4; Fig. S2 to Fig. S4),
388 which are indicators of photochemical processing of emissions.

389 However, as initially discussed by Nault et al. (2018) and shown in Fig. 4, there is large
390 variability in these various metrics across the urban areas evaluated here. To the best of the
391 authors' knowledge, this variability has not been explored and its physical meaning has not been
392 interpreted. As shown in Fig. 4, though, the trends in $\Delta SOA/\Delta CO$ are similar to the trends in the
393 slopes of SOA versus O_x , PAN, or HCHO. For example, Seoul is the highest for nearly all
394 metrics, and is approximately a factor of 6 higher than the urban area, Houston, that generally



395 showed the lowest photochemical metrics. This suggests that the variability is related to a
396 physical factor, including emissions and chemistry.

397 The VOC concentration, together with how quickly the emitted VOCs react ($\sum k_i \times [\text{VOC}]_i$,
398 i.e., the hydroxyl radical, or OH, reactivity of VOCs), where k is the OH rate coefficient for each
399 VOC, are a determining parameter for ASOA formation over urban spatial scales (Eq. 8). ASOA
400 formation is normalized here to the excess CO mixing ratio (ΔCO) to account for the effects of
401 meteorology, dilution, and non-urban background levels, and allow for easier comparison
402 between different studies:

$$403 \quad \frac{\Delta \text{ASOA}}{\Delta \text{CO}} \propto [\text{OH}] \times \Delta t \times \left(\sum_i k_i \times \left[\frac{\text{VOC}}{\text{CO}} \right]_i \times Y_i \right) \quad \text{Eq. 8}$$

404 where Y is the aerosol yield for each compound (mass of SOA formed per unit mass of precursor
405 reacted), and $[\text{OH}] \times \Delta t$ is the PA.

406 BTEX are one group of known ASOA precursors (Gentner et al., 2012; Hayes et al.,
407 2013), and their emission ratio (to CO) was determined for all campaigns (Table S5). BTEX can
408 thus provide insight into ASOA production. Fig. 5a shows that the variation in ASOA (at PA =
409 0.5 equivalent days) is highly correlated with the emission reactivity ratio of BTEX (R_{BTEX} ,
410 $\sum_i [\text{VOC}/\text{CO}]_i$) across all the studies. However, BTEX alone cannot account for much of the
411 ASOA formation (see budget closure discussion below), and instead, BTEX may be better
412 thought of as both partial contributors and also as indicators for the co-emission of other
413 (unmeasured) organic precursors that are also efficient at forming ASOA.

414 O_x , PAN, and HCHO are produced from the oxidation of a much wider set of VOC
415 precursors (including small alkenes, which do not appreciably produce SOA when oxidized).



416 These alkenes have similar reaction rate constants with OH as the most reactive BTEX
417 compounds (Table S11); however, their emissions and concentration can be higher than BTEX
418 (Table S7). Thus, alkenes would dominate R_{Total} , leading to O_x , HCHO, and PAN being produced
419 more rapidly than ASOA (Fig. 5b–d). When R_{BTEX} becomes more important for R_{Total} , the emitted
420 VOCs are more efficient in producing ASOA. Thus, the ratio of ASOA to gas-phase
421 photochemical products shows a strong correlation with $R_{\text{BTEX}}/R_{\text{Total}}$ (Fig. 5b–d).

422

423 **3.2 Budget Closure of ASOA for 4 Urban Areas on 3 Continents Indicates Reasonable** 424 **Understanding of ASOA Sources**

425 We show that BTEX alone cannot explain the observed ASOA budget for urban areas
426 around the world. Fig. 6a shows that approximately $25 \pm 6\%$ of the observed ASOA originates
427 from the photooxidation of BTEX. Therefore, other precursors must account for most of the
428 ASOA produced.

429 Because alkanes, alkenes, and oxygenated compounds with carbon numbers less than 6
430 are not significant ASOA precursors, we focus on emissions and sources of BTEX, other
431 mono-aromatics, IVOCs, and SVOCs. These three classes of VOCs, aromatics, IVOCs, and
432 SVOCs, have been suggested to be significant ASOA precursors in urban atmospheres
433 (Robinson et al., 2007; Hayes et al., 2015; Ma et al., 2017; McDonald et al., 2018; Nault et al.,
434 2018; Schroder et al., 2018; Shah et al., 2018), originating from both fossil fuel and VCP
435 emissions.

436 Using the best available emission inventories from cities on three continents
437 (EMEP/EEA, 2016; McDonald et al., 2018; Li et al., 2019) and observations, we quantify the



438 emissions of BTEX, other mono-aromatics, IVOCs, and SVOCs for both fossil fuel (e.g.,
439 gasoline, diesel, kerosene, etc.), VCPs (e.g., coatings, inks, adhesives, personal care products,
440 and cleaning agents), and cooking sources (Fig. 2 and Fig. 3). This builds off the work of
441 McDonald et al. (2018) for urban regions on three different continents. Combining these
442 inventories and observations for the various locations provide the following insights about the
443 potential ASOA precursors not easily measured or quantified in urban environments (e.g., Zhao
444 et al., 2014; Lu et al., 2018): (1) aromatics from fossil fuel accounts for 14-40% (mean 22%) of
445 the total BTEX and IVOC emissions for the five urban areas investigated in-depth (Fig. 2),
446 agreeing with prior studies that have shown that the observed ASOA cannot be reconciled by the
447 observations or emission inventory of aromatics from fossil fuels (e.g., Ensberg et al., 2014;
448 Hayes et al., 2015). (2) BTEX from both fossil fuels and VCPs account for 25-95% (mean 43%)
449 of BTEX and IVOC emissions (Fig. 2). China has the lowest contribution of IVOCs, potentially
450 due to differences in chemical make-up of the solvents used daily (Li et al., 2019), but more
451 research is needed to investigate the differences in IVOCs:BTEX from Beijing versus US and
452 UK emission inventories. Nonetheless, this shows the importance of IVOCs for both emissions
453 and ASOA precursors. (3) IVOCs are generally equal to, if not greater than, the emissions of
454 BTEX in 4 of the 5 urban areas investigated here (Fig. 2). (4) Overall, VCPs account for a large
455 fraction of the BTEX and IVOC emissions for all five cities. (5) Finally, SVOCs account for
456 27-88% (mean 53%) of VOCs generally considered ASOA precursors (VOCs with volatility
457 saturation concentrations $\leq 10^7 \mu\text{g m}^{-3}$) (Fig. 3). Beijing has the highest contribution of SVOCs
458 to ASOA precursors due to the use of solid fuels and cooking emissions (Hu et al., 2016). Also,
459 this indicates the large contribution of a class of VOCs difficult to measure (Robinson et al.,



460 2007) that are an important ASOA precursor (e.g., Hayes et al., 2015), showing further emphasis
461 should be placed in quantifying the emissions of this class of compounds.

462 These results provide an ability to further investigate the mass balance of predicted and
463 observed ASOA for these urban locations (Fig. 6). The inclusion of IVOCs, other aromatics not
464 including BTEX, and SVOCs leads to the ability to explain, on average, $85\pm 12\%$ of the observed
465 ASOA for these urban locations around the world (Fig. 6a). Further, VCP contribution to ASOA
466 is important for all these urban locations, accounting for, on average, $37\pm 3\%$ of the observed
467 ASOA (Fig. 6b).

468 This bottom-up mass budget analysis provides important insights to further explain the
469 correlation observed in Fig. 5. First, IVOCs are generally co-emitted from similar sources as
470 BTEX for the urban areas investigated in-depth (Fig. 2). The oxidation of these co-emitted
471 species leads to the ASOA production observed across the urban areas around the world. Second,
472 S/IVOCs generally have similar rate constants as toluene and xylenes ($\geq 1 \times 10^{-11} \text{ cm}^3 \text{ molec.}^{-1} \text{ s}^{-1}$)
473 (Zhao et al., 2014, 2017), the compounds that contribute the most to R_{BTEX} , explaining the rapid
474 ASOA production that has been observed in various studies (de Gouw and Jimenez, 2009;
475 DeCarlo et al., 2010; Hayes et al., 2013; Hu et al., 2013, 2016; Nault et al., 2018; Schroder et al.,
476 2018) and correlation (Fig. 5). Finally, the contribution of VCPs and fossil fuel sources to ASOA
477 is similar across the cities, expanding upon and further supporting the conclusion of McDonald
478 et al. (2018) in the importance of identifying and understanding VCP emissions in order to
479 explain ASOA.

480

481 **4. Improved Urban SIMPLE Model Using Multi-Cities to Constrain**



482 4.1 Updates to the SIMPLE Model

483 With the combination of the new dataset, which expands across urban areas on three
484 continents, the SIMPLE parameterization for ASOA (Hodzic and Jimenez, 2011) is updated in
485 the standard GEOS-Chem model to reproduce observed ASOA in Fig. 5a. The parameterization
486 operates as represented by Eq. 9.



488 SOAP represents the lumped precursors of ASOA, k is the reaction rate coefficient with OH
489 ($1.25 \times 10^{-11} \text{ cm}^3 \text{ molecules}^{-1} \text{ s}^{-1}$), and $[\text{OH}]$ is the OH concentration in molecules cm^{-3} .

490 SOAP emissions were calculated based on the relationship between $\Delta\text{SOA}/\Delta\text{CO}$ and
491 $R_{\text{aromatics}}/\Delta\text{CO}$ in Fig. 5a. First, we calculated $R_{\text{aromatics}}/\Delta\text{CO}$ (Eq. 10) for each grid cell and time
492 step as follows:

$$493 \quad \frac{R_{\text{aromatics}}}{\Delta\text{CO}} = \frac{E_{\text{B}} \times k_{\text{B}} + E_{\text{T}} \times k_{\text{T}} + E_{\text{X}} \times k_{\text{X}}}{E_{\text{CO}}} \quad \text{Eq. 10}$$

494 Where E and k stand for the emission rate and reaction rate coefficient with OH, respectively, for
495 benzene (B), toluene (T), and xylenes (X). Ethylbenzene was not included in this calculation
496 because its emission was not available in HTAPv2 emission inventory. However, ethylbenzene
497 contributed a minor fraction of the mixing ratio ($\sim 7\%$, Table S5) and reactivity ($\sim 6\%$) of the
498 total BTEX across the campaigns. Reaction rate constants used in this study were 1.22×10^{-12} ,
499 5.63×10^{-12} , and $1.72 \times 10^{-11} \text{ cm}^3 \text{ molec.}^{-1} \text{ s}^{-1}$ for benzene, toluene, and xylene, respectively
500 (Atkinson and Arey, 2003; Atkinson et al., 2006).



501 Second, $E_{\text{SOAP}}/E_{\text{CO}}$ can be obtained from the result of Eq. 11, using slope and intercept in
502 Fig. 5a, with a correction factor (F) to consider additional SOA production after 0.5 PA
503 equivalent days, since Fig. 5a shows the comparison at 0.5 PA equivalent days.

$$504 \quad \frac{E_{\text{SOAP}}}{E_{\text{CO}}} = \left(\text{Slope} \times \frac{R_{\text{Aromatics}}}{\Delta \text{CO}} + \text{Intercept} \right) \times F \quad \text{Eq. 11}$$

505 Where slope is 24.8 and intercept is -1.7 from Fig. 5a. F (Eq. 12) can be calculated as follows:

$$506 \quad F = \frac{ASOA_{t=\infty}}{ASOA_{t=0.5d}} = \frac{SOAP_{t=0}}{SOAP_{t=0} \times (1 - \exp(-k \times \Delta t \times [\text{OH}])), \Delta t = 43200 \text{ s}} \quad \text{Eq. 12}$$

507 F was calculated as 1.8 by using $[\text{OH}] = 1.5 \times 10^6 \text{ molecules cm}^{-3}$, which was used in the
508 definition of 0.5 PA equivalent days for Fig. 5a.

509 Finally, E_{SOAP} can be computed by multiplying CO emissions (E_{CO}) for every grid point
510 and time step in GEOS-Chem by the $E_{\text{SOAP}}/E_{\text{CO}}$ ratio.

511

512 4.2 Results of Updated SIMPLE Model

513 The SIMPLE model was originally designed and tested against the observations collected
514 around Mexico City (Hodzic and Jimenez, 2011). It was then tested against observations
515 collected in Los Angeles (Hayes et al., 2015; Ma et al., 2017). As both data sets have nearly
516 identical $\Delta \text{SOA}/\Delta \text{CO}$ and R_{BTEX} (Fig. 4 and Fig. 5), it is not surprising that the SIMPLE model
517 did well in predicting the observed $\Delta \text{SOA}/\Delta \text{CO}$ for these two urban regions with consistent
518 parameters. Though the SIMPLE model generally performed better than more explicit models, it
519 generally had lower skill in predicting the observed ASOA in urban regions outside of Mexico
520 City and Los Angeles (Shah et al., 2019; Pai et al., 2020).



521 This may stem from the original SIMPLE model with constant parameters missing the
522 ability to change the amount and reactivity of the emissions, which are different for the various
523 urban regions, versus the ASOA precursors being emitted proportionally to only CO (Hodzic and
524 Jimenez, 2011; Hayes et al., 2015). For example, in the HTAP emissions inventory, the CO
525 emissions for Seoul, Los Angeles, and Mexico City are all similar (Fig. S6); thus, the original
526 SIMPLE model would suggest similar $\Delta\text{SOA}/\Delta\text{CO}$ for all three urban locations. However, as
527 shown in Fig. 4 and Fig. 5, the $\Delta\text{SOA}/\Delta\text{CO}$ is different by nearly a factor of 2. The inclusion of
528 the emissions and reactivity, where R_{BTEX} for Seoul is approximately a factor of 2.5 higher than
529 Los Angeles and Seoul, into the improved SIMPLE model better accounts for the variability in
530 SOA production, as shown in Fig. 5. Thus, the inclusion and use of this improved SIMPLE
531 model refines the simplified representation of ASOA in chemical transport models and/or box
532 models.

533

534 **5. Preliminary Evaluation of Worldwide Premature Deaths Due to ASOA with Updated** 535 **SIMPLE Parameterization**

536 The improved SIMPLE parameterization is used along with GEOS-Chem to provide an
537 accurate estimation of ASOA formation in urban areas worldwide and provide an ability to
538 obtain realistic simulations of ASOA based on measurement data. We use this model to quantify
539 the attribution of $\text{PM}_{2.5}$ ASOA to premature deaths. Analysis up to this point has been for PM_1 ;
540 however, both the chemical transport model and epidemiological studies utilize $\text{PM}_{2.5}$. For
541 ASOA, this will not impact the discussion and results here because the mass of OA (typically
542 80–90%) is dominated by PM_1 (e.g., Bae et al., 2006; Seinfeld and Pandis, 2006), and ASOA is



543 formed mostly through condensation of oxidized species, which favors partitioning onto smaller
544 particles (Seinfeld and Pandis, 2006).

545 The procedure for this analysis is described in Fig. 7 and Sect. 2.5 and 2.6. Briefly, we
546 combine high-resolution satellite-based $PM_{2.5}$ estimates (for exposure) and a chemical transport
547 model (GEOS-Chem, for fractional composition) to estimate ASOA concentrations and various
548 sensitivity analysis (van Donkelaar et al., 2015). We calculated ~3.3 million premature deaths
549 (using the Integrated Exposure-Response, IER, function) are due to long-term exposure of
550 ambient $PM_{2.5}$ (Fig. S7, Table S14), consistent with recent literature (Cohen et al., 2017).

551 The attribution of ASOA $PM_{2.5}$ premature deaths can be calculated one of two ways: (a)
552 marginal method (Silva et al., 2016) or (b) attributable fraction method (Anenberg et al., 2019).
553 For method (a), it is assumed that a fraction of the ASOA is removed, keeping the rest of the
554 $PM_{2.5}$ components approximately constant, and the change in deaths is calculated from the deaths
555 associated with the total concentration less the deaths calculated using the reduced total $PM_{2.5}$
556 concentrations. For method (b), the health impact is attributed to each $PM_{2.5}$ component by
557 multiplying the total deaths by the fractional contribution of each component to total $PM_{2.5}$. For
558 method (a), the deaths attributed to ASOA are ~340,000 people per year (Fig. 8); whereas, for
559 method (b), the deaths are ~370,000 people per year. Both of these are based on the IER response
560 function (Cohen et al., 2017).

561 Additional recent work (Burnett et al., 2018) has suggested less reduction in the
562 premature deaths versus $PM_{2.5}$ concentration relationship at higher $PM_{2.5}$ concentrations, and
563 lower concentration limits for the threshold below which this relationship is negligible, both of
564 which lead to much higher estimates of $PM_{2.5}$ associated premature deaths. This is generally



565 termed the Global Exposure Mortality Model (GEMM). Using the two attribution methods
566 described above (a and b), the ASOA $PM_{2.5}$ premature deaths are estimated to be ~640,000
567 (method a) and ~900,000 (method b) (Fig. S7 and Fig. S10 and Table S15).

568 Compared to prior studies using chemical transport models to estimate premature deaths
569 associated with ASOA (e.g., Silva et al., 2016; Ridley et al., 2018), which assumed non-volatile
570 POA and “traditional” ASOA precursors, the attribution of premature mortality due to ASOA is
571 over an order of magnitude higher in this study (Fig. 9). This occurs using either the IER and
572 GEMM approach for estimating premature mortality (Fig. 9). For regions with larger populations
573 and more $PM_{2.5}$ pollution, the attribution is between a factor of 40 to 80 higher. This stems from
574 the non-volatile POA and “traditional” ASOA precursors over-estimating POA and
575 under-estimating ASOA compared to observations (Schroder et al., 2018). These offsetting
576 errors will lead to model predicted total OA similar to observations (Ridley et al., 2018; Schroder
577 et al., 2018), yet different conclusions on whether POA versus SOA is more important for
578 reducing $PM_{2.5}$ associated premature mortality. Using a model constrained to atmospheric
579 observations (Fig. 5 and Fig. 6, see Sect. 4) leads to a more accurate estimation of the
580 contribution of ASOA to $PM_{2.5}$ associated premature mortality that has not been possible in prior
581 studies. We note that ozone concentrations change little as we change the ASOA simulation (see
582 Sect. S4 in the SI and Fig. S12).

583 A limitation in this study is the lack of sufficient measurements in South and Southeast
584 Asia, Eastern Europe, Africa, and South America (Fig. 1), though these areas account for 44% of
585 the predicted reduction in premature mortality for the world (Table S14). However, as
586 highlighted in Table S16, these regions likely still consume both transportation fuels and VCPs,



587 although in lower per capita amounts than more industrialized countries. This consumption is
588 expected to lead to the same types of emissions as for the cities studied here, though more field
589 measurements are needed to validate global inventories of VOCs and resulting oxidation
590 products in the developing world. Transportation emissions of VOCs are expected to be more
591 dominant in the developing world due to higher VOC emission factors associated with inefficient
592 combustion engines, such as two-stroke scooters (Platt et al., 2014) and auto-rickshaws (e.g.,
593 Goel and Guttikunda, 2015). Also, unlike many of the cities studied here, solid fuels are used for
594 residential heating and cooking, which impact the outdoor air quality as well (Hu et al., 2013,
595 2016; Lacey et al., 2017; Stewart et al., 2020), and which also lead to SOA (Heringa et al.,
596 2011). Recently, emission factors from Abidjan, Côte d'Ivoire, a developing urban area, showed
597 the dominance of emissions from transportation and solid fuel burning, with BTEX being an
598 important fraction of the total emissions, and that all the emissions were efficient in producing
599 ASOA (Dominutti et al., 2019). Further, investigation of emissions in New Delhi region of India
600 demonstrated the importance of both transportation and solid fuel emissions (Stewart et al.,
601 2020; Wang et al., 2020) while model comparisons with observations show an underestimation
602 of OA compared to observations due to a combination of emissions and OA representation (Jena
603 et al., 2020). Despite emission source differences, SOA is still an important component of $PM_{2.5}$
604 (e.g., Singh et al., 2019) and thus will impact air quality and premature mortality in developing
605 regions. Admittedly, though, our estimates will be less accurate for these regions.

606

607 **6. Conclusions**



608 In summary, ASOA is an important, though inadequately constrained component of air
609 pollution in megacities and urban areas around the world. This stems from the complexity
610 associated with the numerous precursor emission sources, chemical reactions, and oxidation
611 products that lead to observed ASOA concentrations. We have shown here that the variability in
612 observed ASOA across urban areas is correlated with R_{BTEX} , a marker for the co-emissions of
613 IVOC from both transportation and VCP emissions. Global simulations indicate ASOA
614 contributes to a substantial fraction of the premature mortality associated with $\text{PM}_{2.5}$. Reductions
615 of the ASOA precursors will reduce the premature deaths associated with $\text{PM}_{2.5}$, indicating the
616 importance of identifying and reducing exposure to sources of ASOA. These sources include
617 emissions that are both traditional (transportation) as well as non-traditional emissions of
618 emerging importance (VCPs) to ambient $\text{PM}_{2.5}$ concentrations in cities around the world. Further
619 investigation of speciated IVOCs and SVOCs for urban areas around the world along with SOA
620 mass concentration and other photochemical products (e.g., O_x , PAN, and HCHO) for other
621 urban areas, especially in South Asia, throughout Africa, and throughout South America, would
622 provide further constraints to improve the SIMPLE model and our understanding of the emission
623 sources and chemistry that leads to the observed SOA and its impact on premature mortality.



624 Acknowledgements

625

626 This study was partially supported by grants from NASA NNX15AT96G, NNX16AQ26G, Sloan
627 Foundation 2016-7173, NSF AGS-1822664, EPA STAR 83587701-0, NERC NE/H003510/1,
628 NERC NE/H003177/1, NERC NE/H003223/1, NOAA NA17OAR4320101, NCAS
629 R8/H12/83/037, Natural Science and Engineering Research Council of Canada (NSERC,
630 RGPIN/05002-2014), and the Fonds de Recherche du Québec —Nature et technologies
631 (FRQNT, 2016-PR-192364). This manuscript has not been formally reviewed by EPA. The
632 views expressed in this document are solely those of the authors and do not necessarily reflect
633 those of the Agency. EPA does not endorse any products or commercial services mentioned in
634 this publication. We thank Katherine Travis for useful discussions. We acknowledge B. J. Bandy,
635 J. Lee, G. P. Mills, D. D. Montzka, J. Stutz, A. J. Weinheimer, E. J. Williams, E. C. Wood, and D.
636 R. Worsnop for use of their data.

637

638 Data Availability

639 TexAQS measurements are available at
640 <https://esrl.noaa.gov/csl/groups/csl7/measurements/2000TexAQS/LaPorte/DataDownload/> and
641 upon request. NEAQS measurements are available at
642 <https://www.esrl.noaa.gov/csl/groups/csl7/measurements/2002NEAQS/>. MILAGRO
643 measurements are available at <http://doi.org/10.5067/Aircraft/INTEXB/Aerosol-TraceGas>.
644 CalNex measurements are available at
645 <https://esrl.noaa.gov/csl/groups/csl7/measurements/2010calnex/Ground/DataDownload/>.
646 ClearfLo measurements are available at
647 <https://catalogue.ceda.ac.uk/uuid/6a5f9eedd68f43348692b3bace3eba45>. SEAC⁴RS measurements
648 are available at <http://doi.org/10.5067/Aircraft/SEAC4RS/Aerosol-TraceGas-Cloud>. WINTER
649 measurements are available at https://data.eol.ucar.edu/master_lists/generated/winter/.
650 KORUS-AQ measurements are available at
651 <http://doi.org/10.5067/Suborbital/KORUSAQ/DATA01>. Data from Chinese campaigns are
652 available upon request, and rest of data used were located in papers cited. GEOS-Chem data
653 available upon request. Figures will become accessible at
654 cires1.colorado.edu/jimenez/group_pubs.html.

655

656 Competing Interests

657 The authors declare no competing interests.

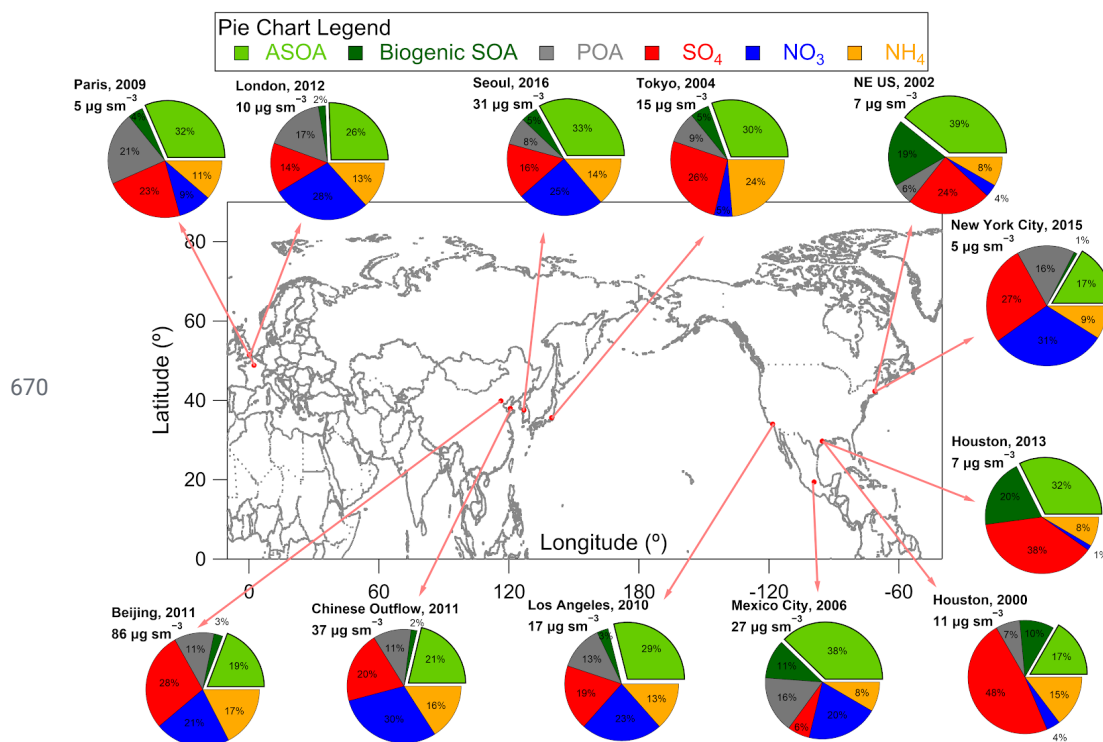
658

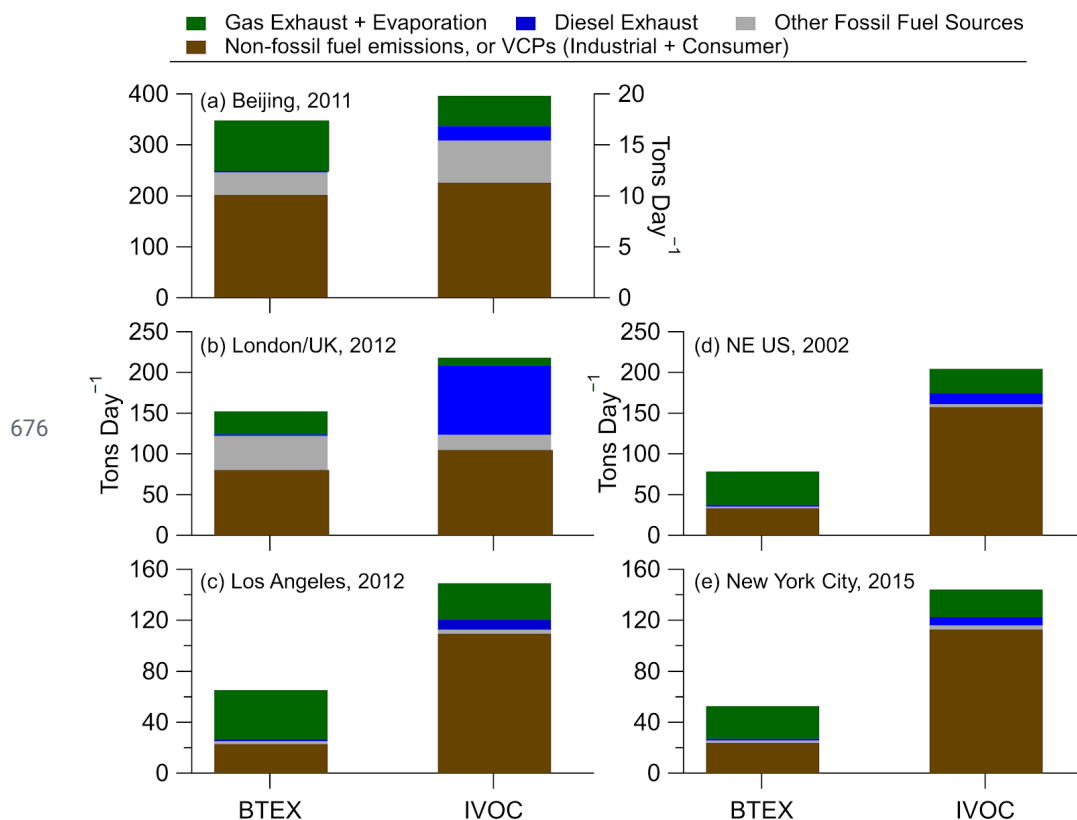
659 Author Contribution

660 B.A.N., D.S.J., B.C.M., J.A.dG., and J.L.J designed the experiment and wrote the paper. B.A.N.,
661 P.C.-J., D.A.D., W.H., J.C.S., J.A., D.R.B., M.R.C., H.C., M.M.C., P.F.D., G.S.D., R.D., F.F., A.F.,
662 J.B.G., G.G., J.F.H., T.F.H., P.L.H., J.H., M.H., L.G.H., B.T.J., W.C.K., J.L., I.B.P., J.P., B.R.,



663 C.E.R., D.R., J.M.R., T.B.R, M.S., J.W., C.W., P.W., G.M.W., D.E.Y., B.Y., J.A.dG., and J.L.J.
664 collected and analyzed the data. D.S.J. and A.H. ran the GEOS-Chem model and B.A.N., D.S.J,
665 and J.L.J. analyzed the model output. B.A.N., P.L.H., J.M.S., and J.L.J. ran and analyzed the 0-D
666 model used for ASOA budget analysis of ambient observations. B.C.M., A.L., M.L., and Q.Z.
667 analyzed and provided the emission inventories used for the 0-D box model. D.S.J., D.K.H., and
668 M.O.N. conducted the ASOA attribution to mortality calculation, and B.A.N., D.S.J., D.K.H.,
669 M.O.N., J.A.dG, and J.L.J analyzed the results. All authors reviewed the paper.

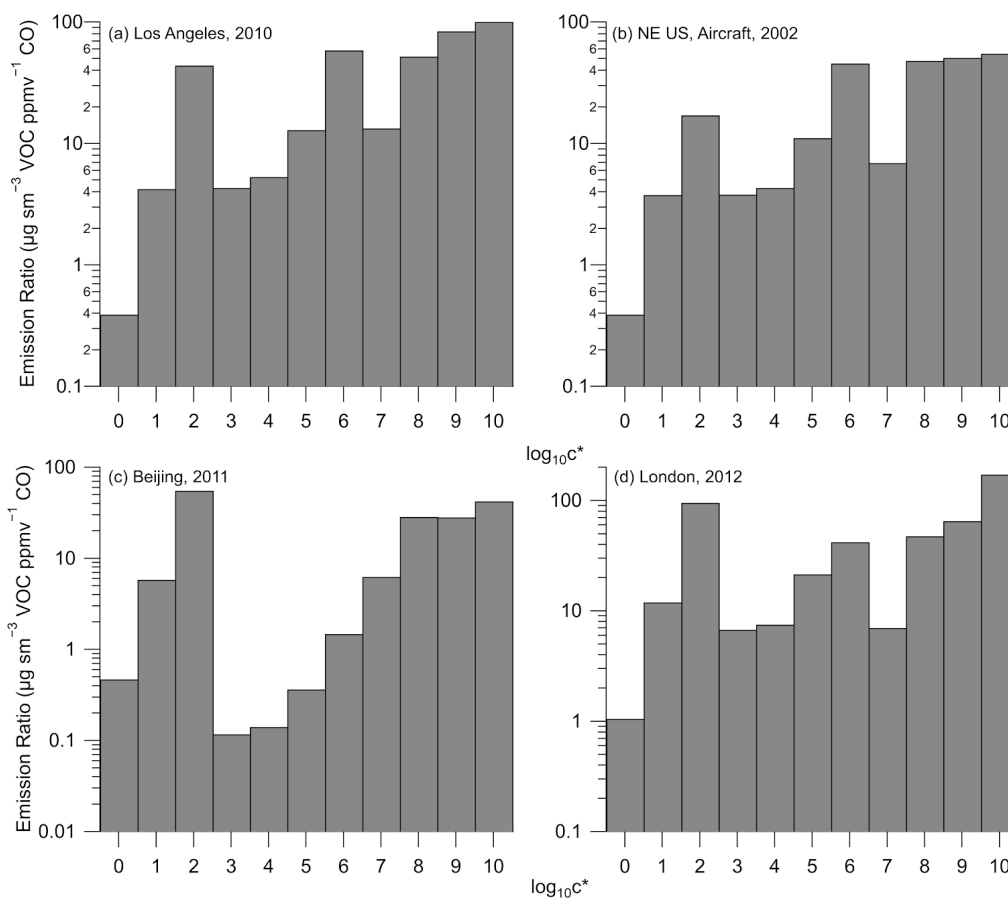




677 **Figure 2.** Comparison of BTEX and IVOC sources for (a) Beijing (see SI section about Beijing
678 emission inventory), (b) London (see SI section about London/UK emission inventory), and (c)
679 Los Angeles, (d) Northeast United States, and (e) New York City (see SI section about United
680 States for (c) – (e)). For (a), BTEX is on the left axis and IVOC is on the right axis, due to the
681 small emissions per day for IVOC.

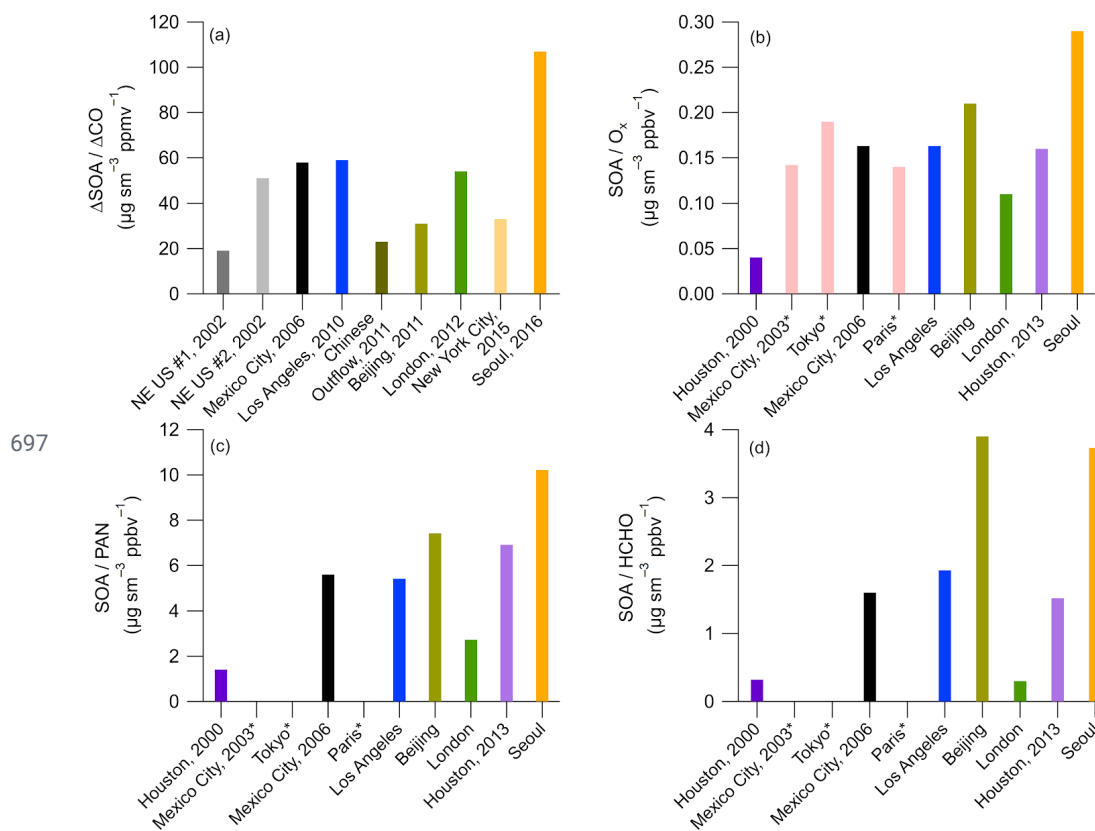


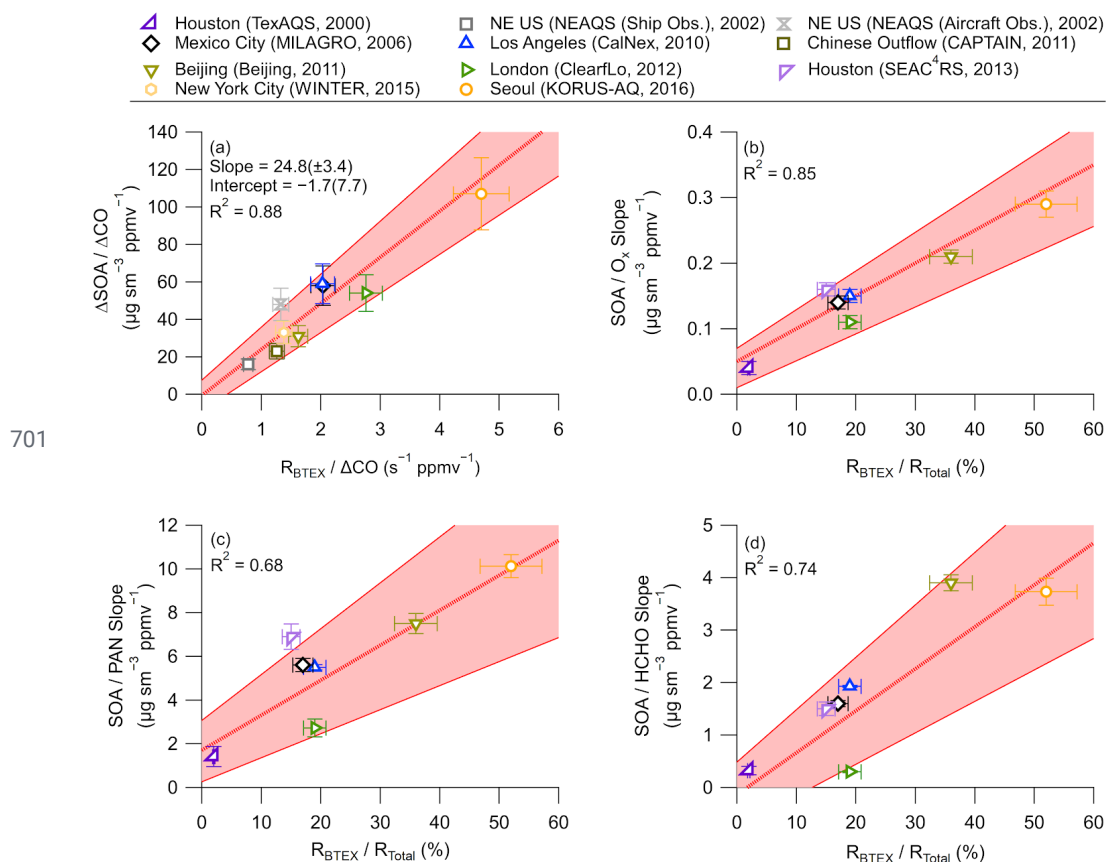
682



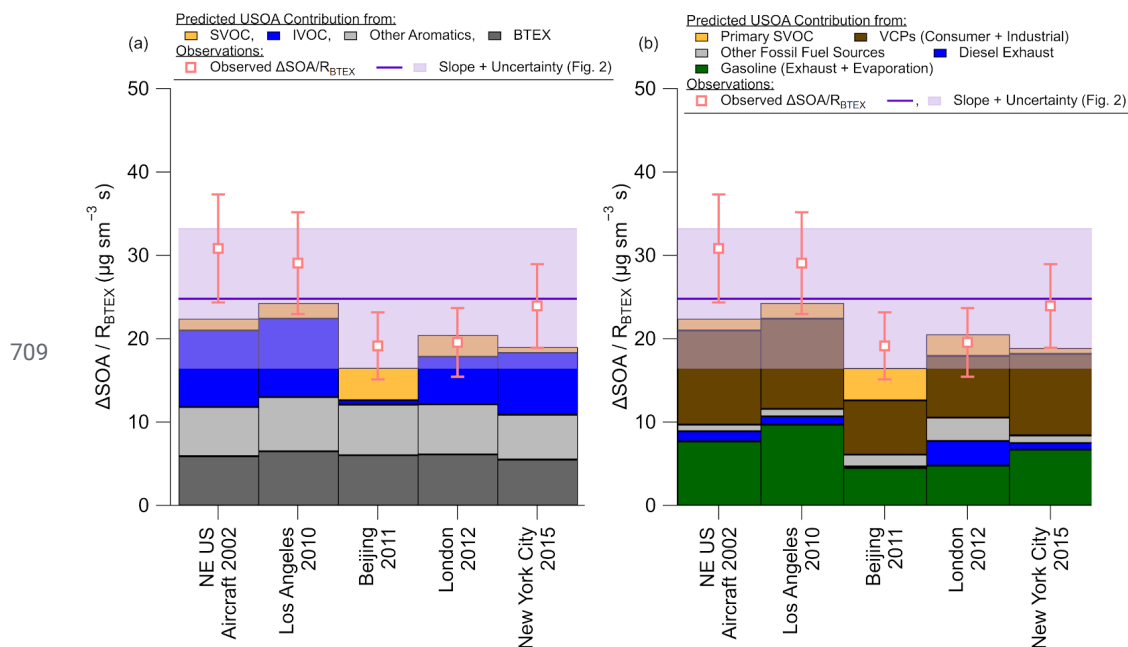
683

684 **Figure 3.** Emission ratio versus saturation concentration ($\log_{10}(c^*)$) for (a) Los Angeles, (b) NE
685 US, aircraft, (c) Beijing, and (d) London. The emission ratios for VOCs ($\log_{10}(c^*) \geq 7$) were
686 taken from de Gouw et al. (2017) and Ma et al. (2017) for Los Angeles, Warneke et al. (2007) for
687 NE US, aircraft, and Wang et al. (2014) for Beijing while the VOC emission ratio for London is
688 from Table S6 to Table S8. For VOCs between $\log_{10}(c^*)$ of 3 and 6 (IVOCs), the volatility
689 distribution from McDonald et al. (2018), along with the ratio of IVOC to BTEX from Figure
690 SI-6 and the emission ratio of BTEX (Table S6), were used to determine the emission ratio
691 versus saturation concentration. Finally, for VOCs between $\log_{10}(c^*)$ 0 and 2 (SVOCs), the
692 volatility distributions from Robinson et al. (2007) for non-fossil fuel POA and from Worton et
693 al. (2014) for fossil fuel POA were used to convert the normalized POA mass concentration
694 (Table S9) to VOC emission ratios. Note, the emission ratio versus saturation concentration for
695 New York City, 2015, was similar to (b), as the emissions were similar (Fig. 2) and the BTEX for
696 New York City is the same as NE US (Table S5).





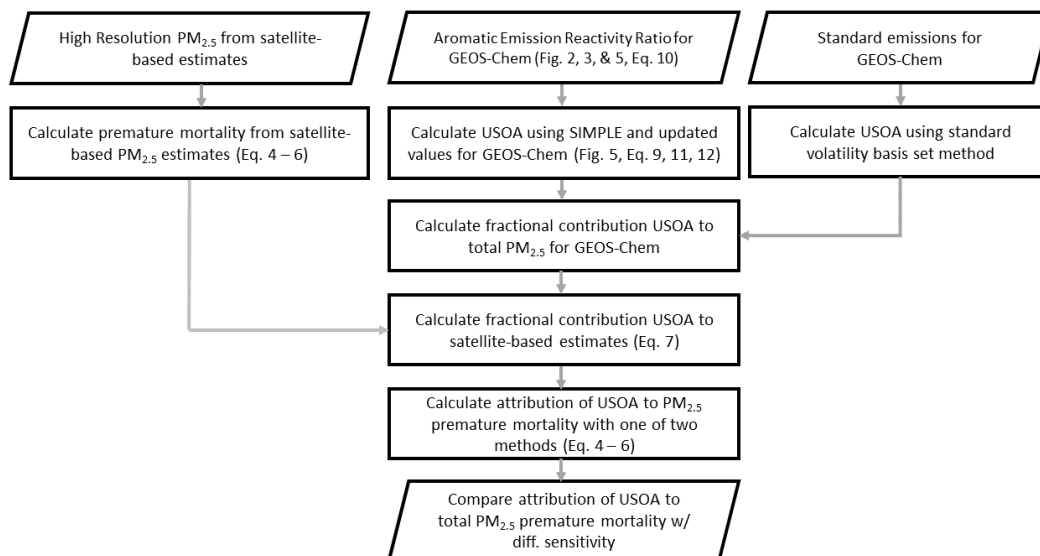
702 **Figure 5.** (a) Scatter plot of background and dilution corrected ASOA concentrations
 703 ($\Delta\text{ASOA}/\Delta\text{CO}$ at $\text{PA} = 0.5$ equivalent days) versus BTEX emission reactivity ratio ($R_{\text{BTEX}} =$
 704 $\sum_i [\text{VOC}/\text{CO}]_i$) for multiple major field campaigns on three continents. Comparison of ASOA
 705 versus (b) Ox, (c) PAN, and (d) HCHO slopes versus the ratio of the BTEX/Total emission
 706 reactivity, where total is the OH reactivity for the emissions of BTEX + C-2-3 alkenes + C2-6
 707 alkanes (Table S5 through Table S7), for the campaigns studied here. For all figures, red shading
 708 is the $\pm 1\sigma$ uncertainty of the slope, and the bars are $\pm 1\sigma$ uncertainty of the data (see Sect. 2.2).



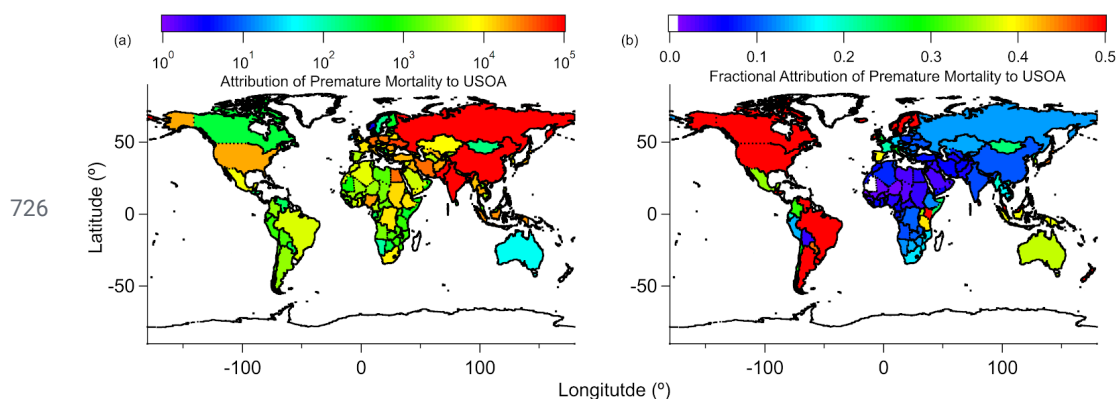
710 **Figure 6.** (a) Budget analysis for the contribution of the observed $\Delta SOA/R_{BTEX}$ (Fig. 5) for cities
 711 with known emissions inventories for different volatility classes (see SI and Fig. 2 and Fig. 3).
 712 (b) Same as (a), but for sources of emissions. For (a) and (b), SVOC is the contribution from
 713 both vehicle and other (cooking, etc.) sources. See Sect. 2 and SI for information about the
 714 emissions, ASOA precursor contribution, error analysis, and discussion about sensitivity of
 715 emission inventory IVOC/BTEX ratios for different cities and years in the US.



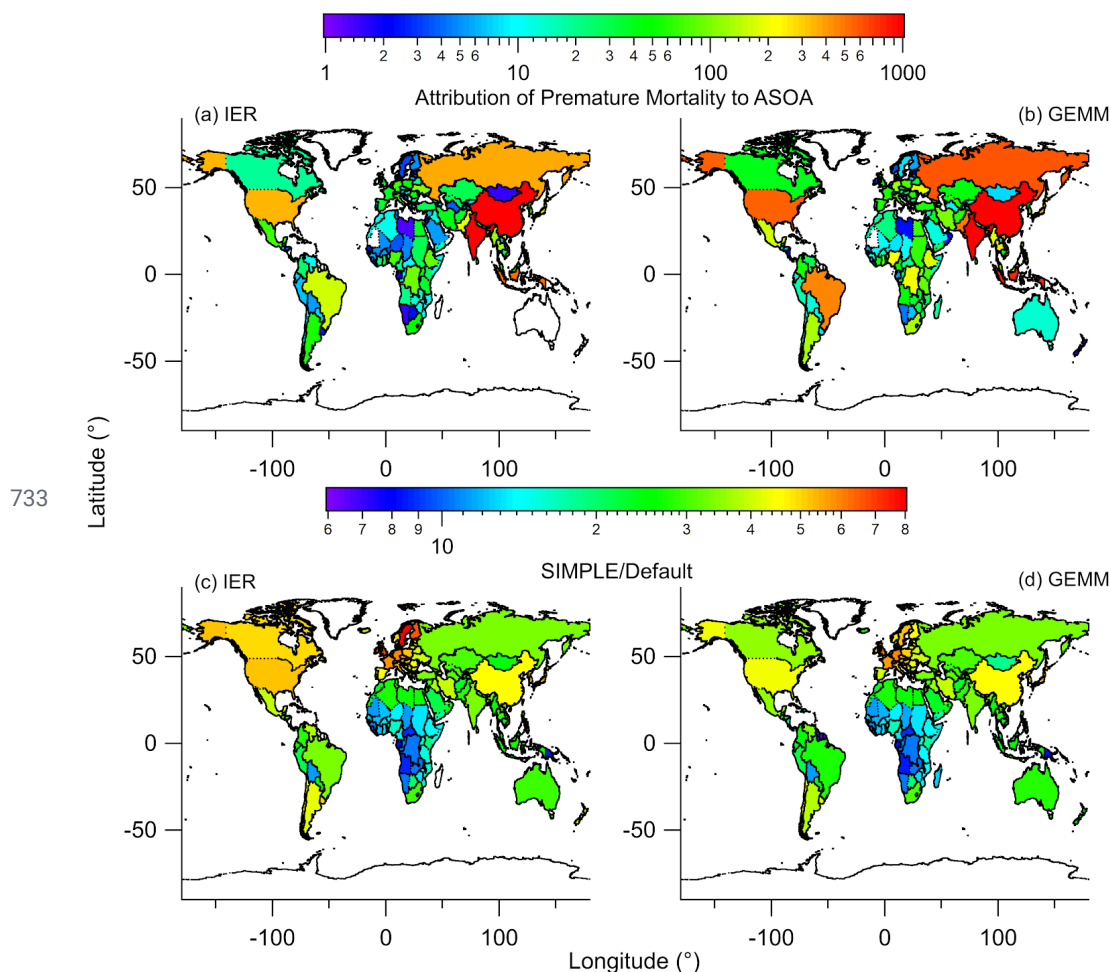
716



717 **Figure 7.** Flowchart describing how observed ASOA production was used to calculate ASOA in
718 GEOS-Chem, and how the satellite-based $PM_{2.5}$ estimates and GEOS-Chem $PM_{2.5}$ speciation was
719 used to estimate the premature mortality and attribution of premature mortality by ASOA. See
720 Sect. 2 for further information about the details in the figure. SIMPLE is described in Eq. 9 and
721 by Hodzic and Jimenez (2011) and Hayes et al. (2015). The one of two methods mentioned
722 include either the Integrated Exposure-Response (IER) (Burnett et al., 2014) with Global Burden
723 of Disease (GBD) dataset (IHME, 2016) or the new Global Exposure Mortality Model (GEMM)
724 (Burnett et al., 2018) methods. For both IER and GEMM, the marginal method (Silva et al.,
725 2016) or attributable fraction method (Anenberg et al., 2019) are used.



727 **Figure 8.** Five-year average (a) estimated reduction in $PM_{2.5}$ -associated premature deaths, by
728 country, upon removing ASOA from total $PM_{2.5}$, and (b) fractional reduction (reduction $PM_{2.5}$
729 premature deaths / total $PM_{2.5}$ premature deaths) in $PM_{2.5}$ -associated premature deaths, by
730 country, upon removing ASOA from GEOS-Chem. The IER methods are used here. See Fig. S7
731 and Fig. S10 for results using GEMM. See Fig. S8 for $10 \times 10 \text{ km}^2$ area results in comparison
732 with country-level results.



734 **Figure 9.** Attribution of premature mortality to ASOA using (a) IER or (b) GEMM, using the
735 non-volatile primary OA and traditional SOA precursors method in prior studies (e.g., Ridley et
736 al., 2018). The increase in attribution of premature mortality to ASOA for the “SIMPLE” model
737 (Fig. 8) versus the non-volatile primary OA and traditional SOA precursor method (“Default”),
738 for (c) IER and (d) GEMM.



739 Table 1. List of campaigns used here. For values previously reported for those campaigns, they
 740 are noted. For Seasons, W = Winter, Sp = Spring, and Su = Summer.

Location	Field Campaign	Coordinates		Time Period	Season	Previous Publication/Campaign Overview
		Long. (°)	Lat. (°)			
Houston, TX, USA (2000)	TexAQS 2000	-95.4	29.8	15/Aug/2000 - 15/Sept/2000	Su	Jimenez et al. (2009) ^a , Wood et al. (2010) ^b
Northeast USA (2002)	NEAQS 2002	-78.1 - -70.5	32.8 - 43.1	26/July/2002; 29/July/2002 - 10/Aug/2002	Su	Jimenez et al. (2009) ^a , de Gouw and Jimenez (2009) ^c , Kleinman et al. (2007) ^c
Mexico City, Mexico (2003)	MCMA-2003	-99.2	19.5	31/Mar/2003 - 04/May/2003	Sp	Molina et al. (2007), Herndon et al. (2008) ^b
Tokyo, Japan (2004)		139.7	35.7	24/July/2004 - 14/Aug/2004	Su	Kondo et al. (2008) ^a , Miyakawa et al. (2008) ^a , Morino et al. (2014) ^b
Mexico City, Mexico (2006)	MILAGRO	-99.4 - -98.6	19.0 - 19.8	04/Mar/2006 - 29/Mar/2006	Sp	Molina et al. (2010), DeCarlo et al. (2008) ^a , Wood et al. (2010) ^b , DeCarlo et al. (2010) ^c
Paris, France (2009)	MEGAPOLI	48.9	2.4	13/July/2009 - 29/July/2009	Su	Frenay et al. (2014) ^a , Zhang et al. (2015) ^b
Pasadena, CA, USA (2010)	CalNex	-118.1	34.1	15/May/2010 - 16/June/2010	Sp	Ryerson et al. (2013), Hayes et al. (2013) ^{a,b,c}
Changdao Island, China (2011)	CAPTAIN	120.7	38.0	21/Mar/2011 - 24/Apr/2011	Sp	Hu et al. (2013) ^{a,c}
Beijing, China (2011)	CareBeijing 2011	116.4	39.9	03/Aug/2011 - 15/Sept/2011	Su	Hu et al. (2016) ^{a,b,c}
London, UK (2012)	ClearfLo	0.1	51.5	22/July/2012 - 18/Aug/2012	Su	Bohnenstengel et al. (2015)
Houston, TX, USA (2013)	SEAC ⁴ RS	-96.0 - -94.0	29.2 - 30.3	01/Aug/2013 - 23/Sept/2013	Su	Toon et al. (2016)
New York City, NY, USA (2015)	WINTER	-74.0 - -69.0	39.5 - 42.5	07/Feb/2015	W	Schroder et al. (2018) ^{a,c}
Seoul, South Korea (2016)	KORUS-AQ	124.6 - 128.0	36.8 - 37.6	01/May/2016 - 10/June/2016	Sp	Nault et al. (2018) ^{a,b,c,d}

741 ^aReference used for PM₁ composition. ^bReference used for SOA/O_x slope. ^cReference used for
 742 ΔOA/ΔCO value. ^dReference used for SOA/HCHO and SOA/PAN slopes



743 References

- 744 Anenberg, S., Miller, J., Henze, D. and Minjares, R.: A global snapshot of the air
745 pollution-related health impacts of transportation sector emissions in 2010 and 2015, ICCT,
746 Climate & Clean Air Coalition., 2019.
- 747 Atkinson, R. and Arey, J.: Atmospheric Degradation of Volatile Organic Compounds, Chem.
748 Rev., 103, 4605–4638, 2003.
- 749 Atkinson, R., Baulch, D. L., Cox, R. A., Crowley, J. N., Hampson, R. F., Hynes, R. G., Jenkin,
750 M. E., Rossi, M. J., Troe, J. and IUPAC Subcommittee: Evaluated kinetic and photochemical
751 data for atmospheric chemistry: Volume II - gas phase reactions of organic species, Atmos.
752 Chem. Phys., 6(11), 3625–4055, 2006.
- 753 Bae, M.-S., Demerjian, K. L. and Schwab, J. J.: Seasonal estimation of organic mass to organic
754 carbon in PM_{2.5} at rural and urban locations in New York state, Atmos. Environ., 40(39),
755 7467–7479, 2006.
- 756 Bahreini, R., Ervens, B., Middlebrook, A. M., Warneke, C., de Gouw, J. A., DeCarlo, P. F.,
757 Jimenez, J. L., Brock, C. A., Neuman, J. A., Ryerson, T. B., Stark, H., Atlas, E., Brioude, J.,
758 Fried, A., Holloway, J. S., Peischl, J., Richter, D., Walega, J., Weibring, P., Wollny, A. G. and
759 Fehsenfeld, F. C.: Organic aerosol formation in urban and industrial plumes near Houston and
760 Dallas, Texas, J. Geophys. Res., 114, 1185, 2009.
- 761 Bertram, T. H., Perring, A. E., Wooldridge, P. J., Crouse, J. D., Kwan, A. J., Wennberg, P. O.,
762 Scheuer, E., Dibb, J., Avery, M., Sachse, G., Vay, S. A., Crawford, J. H., McNaughton, C. S.,
763 Clarke, A., Pickering, K. E., Fuelberg, H., Huey, G., Blake, D. R., Singh, H. B., Hall, S. R.,
764 Shetter, R. E., Fried, A., Heikes, B. G. and Cohen, R. C.: Direct Measurements of the Convective
765 Recycling of the Upper Troposphere, Science, 315(5813), 816–820, 2007.
- 766 Bey, I., Jacob, D. J., Yantosca, R. M., Logan, J. A., Field, B. D., Fiore, A. M., Li, Q., Liu, H. Y.,
767 Mickley, L. J. and Schultz, M. G.: Global modeling of tropospheric chemistry with assimilated
768 meteorology: Model description and evaluation, J. Geophys. Res. D: Atmos., 106(D19),
769 23073–23095, 2001.
- 770 Bohnenstengel, S. I., Belcher, S. E., Aiken, A., Allan, J. D., Allen, G., Bacak, A., Bannan, T. J.,
771 Barlow, J. F., Beddows, D. C. S., Bloss, W. J., Booth, A. M., Chemel, C., Coceal, O., Di Marco,
772 C. F., Dubey, M. K., Faloon, K. H., Fleming, Z. L., Furger, M., Gietl, J. K., Graves, R. R., Green,
773 D. C., Grimmond, C. S. B., Halios, C. H., Hamilton, J. F., Harrison, R. M., Heal, M. R., Heard,
774 D. E., Helfter, C., Herndon, S. C., Holmes, R. E., Hopkins, J. R., Jones, A. M., Kelly, F. J.,
775 Kotthaus, S., Langford, B., Lee, J. D., Leigh, R. J., Lewis, A. C., Lidster, R. T., Lopez-Hilfiker,
776 F. D., McQuaid, J. B., Mohr, C., Monks, P. S., Nemitz, E., Ng, N. L., Percival, C. J., Prévôt, A. S.
777 H., Ricketts, H. M. A., Sokhi, R., Stone, D., Thornton, J. A., Tremper, A. H., Valach, A. C.,
778 Visser, S., Whalley, L. K., Williams, L. R., Xu, L., Young, D. E., Zotter, P., Bohnenstengel, S. I.,
779 Belcher, S. E., Aiken, A., Allan, J. D., Allen, G., Bacak, A., Bannan, T. J., Barlow, J. F.,
780 Beddows, D. C. S., Bloss, W. J., Booth, A. M., Chemel, C., Coceal, O., Marco, C. F. D., Dubey,



- 781 M. K., Faloon, K. H., Fleming, Z. L., Furger, M., Gietl, J. K., Graves, R. R., Green, D. C.,
782 Grimmond, C. S. B., Halios, C. H., Hamilton, J. F., Harrison, R. M., Heal, M. R., Heard, D. E.,
783 Helfter, C., Herndon, S. C., Holmes, R. E., Hopkins, J. R., Jones, A. M., Kelly, F. J., Kotthaus,
784 S., Langford, B., Lee, J. D., Leigh, R. J., Lewis, A. C., Lidster, R. T., Lopez-Hilfiker, F. D., et al.:
785 Meteorology, Air Quality, and Health in London: The ClearfLo Project, *Bull. Am. Meteorol.*
786 *Soc.*, 96(5), 779–804, 2015.
- 787 Burnett, R., Chen, H., Szyszkowicz, M., Fann, N., Hubbell, B., Pope, C. A., Apte, J. S., Brauer,
788 M., Cohen, A., Weichenthal, S., Coggins, J., Di, Q., Brunekreef, B., Frostad, J., Lim, S. S., Kan,
789 H., Walker, K. D., Thurston, G. D., Hayes, R. B., Lim, C. C., Turner, M. C., Jerrett, M., Krewski,
790 D., Gapstur, S. M., Diver, W. R., Ostro, B., Goldberg, D., Crouse, D. L., Martin, R. V., Peters, P.,
791 Pinault, L., Tjepkema, M., van Donkelaar, A., Villeneuve, P. J., Miller, A. B., Yin, P., Zhou, M.,
792 Wang, L., Janssen, N. A. H., Marra, M., Atkinson, R. W., Tsang, H., Quoc Thach, T., Cannon, J.
793 B., Allen, R. T., Hart, J. E., Laden, F., Cesaroni, G., Forastiere, F., Weinmayr, G., Jaensch, A.,
794 Nagel, G., Concin, H. and Spadaro, J. V.: Global estimates of mortality associated with long-term
795 exposure to outdoor fine particulate matter, *Proc. Natl. Acad. Sci. U. S. A.*, 115(38), 9592–9597,
796 2018.
- 797 Burnett, R. T., Pope, C. A., Ezzati, M., Olives, C., Lim, S. S., Mehta, S., Shin, H. H., Singh, G.,
798 Hubbell, B., Brauer, M., Anderson, H. R., Smith, K. R., Balmes, J. R., Bruce, N. G., Kan, H.,
799 Laden, F., Prüss-Ustün, A., Turner, M. C., Gapstur, S. M., Diver, W. R. and Cohen, A.: An
800 integrated risk function for estimating the global burden of disease attributable to ambient fine
801 particulate matter exposure, *Environ. Health Perspect.*, 122(4), 397–403, 2014.
- 802 CIESIN: Gridded Population of the World (GPW), v4, SEDAC [online] Available from:
803 <https://sedac.ciesin.columbia.edu/data/collection/gpw-v4> (Accessed 12 May 2020), 2017.
- 804 Coggon, M. M., McDonald, B. C., Vlasenko, A., Veres, P. R., Bernard, F., Koss, A. R., Yuan, B.,
805 Gilman, J. B., Peischl, J., Aikin, K. C., DuRant, J., Warneke, C., Li, S.-M. and de Gouw, J. A.:
806 Diurnal Variability and Emission Pattern of Decamethylcyclopentasiloxane (D₅) from the
807 Application of Personal Care Products in Two North American Cities, *Environ. Sci. Technol.*,
808 52(10), 5610–5618, 2018.
- 809 Cohen, A. J., Brauer, M., Burnett, R., Anderson, H. R., Frostad, J., Estep, K., Balakrishnan, K.,
810 Brunekreef, B., Dandona, L., Dandona, R., Feigin, V., Freedman, G., Hubbell, B., Jobling, A.,
811 Kan, H., Knibbs, L., Liu, Y., Martin, R., Morawska, L., Pope, C. A., Shin, H., Straif, K.,
812 Shaddick, G., Thomas, M., van Dingenen, R., van Donkelaar, A., Vos, T., Murray, C. J. L. and
813 Forouzanfar, M. H.: Estimates and 25-year trends of the global burden of disease attributable to
814 ambient air pollution: an analysis of data from the Global Burden of Diseases Study 2015,
815 *Lancet*, 389(10082), 1907–1918, 2017.
- 816 DeCarlo, P. F., Dunlea, E. J., Kimmel, J. R., Aiken, A. C., Sueper, D., Crouse, J., Wennberg, P.
817 O., Emmons, L., Shinozuka, Y., Clarke, A., Zhou, J., Tomlinson, J., Collins, D. R., Knapp, D.,
818 Weinheimer, A. J., Montzka, D. D., Campos, T. and Jimenez, J. L.: Fast airborne aerosol size and
819 chemistry measurements above Mexico City and Central Mexico during the MILAGRO



- 820 campaign, *Atmos. Chem. Phys.*, 8(14), 4027–4048, 2008.
- 821 DeCarlo, P. F., Ulbrich, I. M., Crounse, J., de Foy, B., Dunlea, E. J., Aiken, A. C., Knapp, D.,
822 Weinheimer, A. J., Campos, T., Wennberg, P. O. and Jimenez, J. L.: Investigation of the sources
823 and processing of organic aerosol over the Central Mexican Plateau from aircraft measurements
824 during MILAGRO, *Atmos. Chem. Phys.*, 10(12), 5257–5280, 2010.
- 825 Dominutti, P., Keita, S., Bahino, J., Colomb, A., Liousse, C., Yoboué, V., Galy-Lacaux, C.,
826 Morris, E., Bouvier, L., Sauvage, S. and Borbon, A.: Anthropogenic VOCs in Abidjan, southern
827 West Africa: from source quantification to atmospheric impacts, *Atmos. Chem. Phys.*, 19(18),
828 11721–11741, 2019.
- 829 van Donkelaar, A., Martin, R. V., Brauer, M. and Boys, B. L.: Use of Satellite Observations for
830 Long-Term Exposure Assessment of Global Concentrations of Fine Particulate Matter, *Environ.*
831 *Health Perspect.*, 123(2), 135–143, 2015.
- 832 van Donkelaar, A., Martin, R. V., Brauer, M., Hsu, N. C., Kahn, R. A., Levy, R. C., Lyapustin,
833 A., Sayer, A. M. and Winker, D. M.: Global Estimates of Fine Particulate Matter using a
834 Combined Geophysical-Statistical Method with Information from Satellites, Models, and
835 Monitors, *Environ. Sci. Technol.*, 50(7), 3762–3772, 2016.
- 836 Duncan Fairlie, T., Jacob, D. J. and Park, R. J.: The impact of transpacific transport of mineral
837 dust in the United States, *Atmos. Environ.*, 41(6), 1251–1266, 2007.
- 838 Dzepina, K., Volkamer, R. M., Madronich, S., Tulet, P., Ulbrich, I. M., Zhang, Q., Cappa, C. D.,
839 Ziemann, P. J. and Jimenez, J. L.: Evaluation of recently-proposed secondary organic aerosol
840 models for a case study in Mexico City, *Atmos. Chem. Phys.*, 9(15), 5681–5709, 2009.
- 841 EMEP/EEA: EMEP/EEA Air Pollutant Emission Inventory Guidebook 2016, EEA,
842 Luxembourg., 2016.
- 843 Ensberg, J. J., Hayes, P. L., Jimenez, J. L., Gilman, J. B., Kuster, W. C., de Gouw, J. A.,
844 Holloway, J. S., Gordon, T. D., Jathar, S., Robinson, A. L. and Seinfeld, J. H.: Emission factor
845 ratios, SOA mass yields, and the impact of vehicular emissions on SOA formation, *Atmos.*
846 *Chem. Phys.*, 14(5), 2383–2397, 2014.
- 847 Freney, E. J., Sellegri, K., Canonaco, F., Colomb, A., Borbon, A., Michoud, V., Crumeyrolle, S.,
848 Amarouche, N., Bourianne, T., Gomes, L., Prevot, A. S. H., Beekmann, M. and
849 Schwarzenböeck, A.: Characterizing the impact of urban emissions on regional aerosol particles:
850 Airborne measurements during the MEGAPOLI experiment, *Atmos. Chem. Phys.*, 14(3),
851 1397–1412, 2014.
- 852 Gentner, D. R., Isaacman, G., Worton, D. R., Chan, A. W. H., Dallmann, T. R., Davis, L., Liu, S.,
853 Day, D. A., Russell, L. M., Wilson, K. R., Weber, R., Guha, A., Harley, R. A. and Goldstein, A.
854 H.: Elucidating secondary organic aerosol from diesel and gasoline vehicles through detailed
855 characterization of organic carbon emissions, *Proc. Natl. Acad. Sci. U. S. A.*, 109(45),



- 856 18318–18323, 2012.
- 857 Goel, R. and Guttikunda, S. K.: Evolution of on-road vehicle exhaust emissions in Delhi, Atmos.
858 Environ., 105, 78–90, 2015.
- 859 de Gouw, J. A. and Jimenez, J. L.: Organic Aerosols in the Earth’s Atmosphere, Environ. Sci.
860 Technol., 43(20), 7614–7618, 2009.
- 861 de Gouw, J. A., Middlebrook, A. M., Warneke, C., Goldan, P. D., Kuster, W. C., Roberts, J. M.,
862 Fehsenfeld, F. C., Worsnop, D. R., Canagaratna, M. R., Pszenny, A. A. P., Keene, W. C.,
863 Marchewka, M., Bertman, S. B. and Bates, T. S.: Budget of organic carbon in a polluted
864 atmosphere: Results from the New England Air Quality Study in 2002, J. Geophys. Res. D:
865 Atmos., 110(16), 1–22, 2005.
- 866 de Gouw, J. A., Gilman, J. B., Kim, S.-W., Lerner, B. M., Isaacman-VanWertz, G., McDonald, B.
867 C., Warneke, C., Kuster, W. C., Lefer, B. L., Griffith, S. M., Dusanter, S., Stevens, P. S. and
868 Stutz, J.: Chemistry of Volatile Organic Compounds in the Los Angeles basin: Nighttime
869 Removal of Alkenes and Determination of Emission Ratios, J. Geophys. Res.: Atmos., 122(21),
870 11,843–11,861, 2017.
- 871 Grieshop, A. P., Logue, J. M., Donahue, N. M. and Robinson, A. L.: Laboratory investigation of
872 photochemical oxidation of organic aerosol from wood fires 1: measurement and simulation of
873 organic aerosol evolution, Atmos. Chem. Phys., 9(4), 1263–1277, 2009.
- 874 Hallquist, M., Wenger, J. C., Baltensperger, U., Rudich, Y., Simpson, D., Claeys, M., Dommen,
875 J., Donahue, N. M., George, C., Goldstein, A. H., Hamilton, J. F., Herrmann, H., Hoffmann, T.,
876 Iinuma, Y., Jang, M., Jenkin, M. E., Jimenez, J. L., Kiendler-Scharr, A., Maenhaut, W.,
877 McFiggans, G., Mentel, T. F., Monod, A., Prévôt, A. S. H., Seinfeld, J. H., Surratt, J. D.,
878 Szmigielski, R. and Wildt, J.: The formation, properties and impact of secondary organic aerosol:
879 current and emerging issues, Atmos. Chem. Phys., 9(14), 5155–5236, 2009.
- 880 Hayes, P. L., Ortega, A. M., Cubison, M. J., Froyd, K. D., Zhao, Y., Cliff, S. S., Hu, W. W.,
881 Toohey, D. W., Flynn, J. H., Lefer, B. L., Grossberg, N., Alvarez, S., Rappenglück, B., Taylor, J.
882 W., Allan, J. D., Holloway, J. S., Gilman, J. B., Kuster, W. C., de Gouw, J. A., Massoli, P.,
883 Zhang, X., Liu, J., Weber, R. J., Corrigan, A. L., Russell, L. M., Isaacman, G., Worton, D. R.,
884 Kreisberg, N. M., Goldstein, A. H., Thalman, R., Waxman, E. M., Volkamer, R., Lin, Y. H.,
885 Surratt, J. D., Kleindienst, T. E., Offenberg, J. H., Dusanter, S., Griffith, S., Stevens, P. S.,
886 Brioude, J., Angevine, W. M. and Jimenez, J. L.: Organic aerosol composition and sources in
887 Pasadena, California, during the 2010 CalNex campaign, J. Geophys. Res. D: Atmos., 118(16),
888 9233–9257, 2013.
- 889 Hayes, P. L., Carlton, A. G., Baker, K. R., Ahmadov, R., Washenfelder, R. A., Alvarez, S.,
890 Rappenglück, B., Gilman, J. B., Kuster, W. C., de Gouw, J. A., Zotter, P., Prévôt, A. S. H.,
891 Szidat, S., Kleindienst, T. E., Ma, P. K. and Jimenez, J. L.: Modeling the formation and aging of
892 secondary organic aerosols in Los Angeles during CalNex 2010, Atmos. Chem. Phys., 15(10),



- 893 5773–5801, 2015.
- 894 Heringa, M. F., DeCarlo, P. F., Chirico, R., Tritscher, T., Dommen, J., Weingartner, E., Richter,
895 R., Wehrle, G., Prévôt, A. S. H. and Baltensperger, U.: Investigations of primary and secondary
896 particulate matter of different wood combustion appliances with a high-resolution time-of-flight
897 aerosol mass spectrometer, *Atmos. Chem. Phys.*, 11(12), 5945–5957, 2011.
- 898 Herndon, S. C., Onasch, T. B., Wood, E. C., Kroll, J. H., Canagaratna, M. R., Jayne, J. T.,
899 Zavala, M. A., Knighton, W. B., Mazzoleni, C., Dubey, M. K., Ulbrich, I. M., Jimenez, J. L.,
900 Seila, R., de Gouw, J. A., de Foy, B., Fast, J., Molina, L. T., Kolb, C. E. and Worsnop, D. R.:
901 Correlation of secondary organic aerosol with odd oxygen in Mexico City, *Geophys. Res. Lett.*,
902 35(15), L15804, 2008.
- 903 Hodzic, A. and Jimenez, J. L.: Modeling anthropogenically controlled secondary organic
904 aerosols in a megacity: A simplified framework for global and climate models, *Geosci. Model
905 Dev.*, 4(4), 901–917, 2011.
- 906 Hodzic, A., Jimenez, J. L., Madronich, S., Aiken, A. C., Bessagnet, B., Curci, G., Fast, J.,
907 Lamarque, J.-F., Onasch, T. B., Roux, G., Schauer, J. J., Stone, E. A. and Ulbrich, I. M.:
908 Modeling organic aerosols during MILAGRO: importance of biogenic secondary organic
909 aerosols, *Atmos. Chem. Phys.*, 9(18), 6949–6981, 2009.
- 910 Hodzic, A., Jimenez, J. L., Prévôt, A. S. H., Szidat, S., Fast, J. D. and Madronich, S.: Can 3-D
911 models explain the observed fractions of fossil and non-fossil carbon in and near Mexico City?,
912 *Atmos. Chem. Phys.*, 10(22), 10997–11016, 2010a.
- 913 Hodzic, A., Jimenez, J. L., Madronich, S., Canagaratna, M. R., DeCarlo, P. F., Kleinman, L. and
914 Fast, J.: Modeling organic aerosols in a megacity: potential contribution of semi-volatile and
915 intermediate volatility primary organic compounds to secondary organic aerosol formation,
916 *Atmos. Chem. Phys.*, 10(12), 5491–5514, 2010b.
- 917 Hu, W., Hu, M., Hu, W., Jimenez, J. L., Yuan, B., Chen, W., Wang, M., Wu, Y., Chen, C., Wang,
918 Z., Peng, J., Zeng, L. and Shao, M.: Chemical composition, sources, and aging process of
919 submicron aerosols in Beijing: Contrast between summer and winter, *J. Geophys. Res. D:*
920 *Atmos.*, 121(4), 1955–1977, 2016.
- 921 Hu, W. W., Hu, M., Yuan, B., Jimenez, J. L., Tang, Q., Peng, J. F., Hu, W., Shao, M., Wang, M.,
922 Zeng, L. M., Wu, Y. S., Gong, Z. H., Huang, X. F. and He, L. Y.: Insights on organic aerosol
923 aging and the influence of coal combustion at a regional receptor site of central eastern China,
924 *Atmos. Chem. Phys.*, 13(19), 10095–10112, 2013.
- 925 IHME: Global Burden of Disease Study 2015 (GBD 2015) Data Resources, GHDx [online]
926 Available from: <http://ghdx.healthdata.org/gbd-2015> (Accessed 2019), 2016.
- 927 Jaeglé, L., Quinn, P. K., Bates, T. S., Alexander, B. and Lin, J.-T.: Global distribution of sea salt
928 aerosols: new constraints from in situ and remote sensing observations, *Atmos. Chem. Phys.*,



- 929 11(7), 3137–3157, 2011.
- 930 Janssen, R. H. H., Tsimpidi, A. P., Karydis, V. A., Pozzer, A., Lelieveld, J., Crippa, M., Prévôt,
931 A. S. H., Ait-Helal, W., Borbon, A., Sauvage, S. and Locoge, N.: Influence of local production
932 and vertical transport on the organic aerosol budget over Paris, *J. Geophys. Res. D: Atmos.*,
933 122(15), 8276–8296, 2017.
- 934 Janssens-Maenhout, G., Crippa, M., Guizzardi, D., Dentener, F., Muntean, M., Pouliot, G.,
935 Keating, T., Zhang, Q., Kurokawa, J., Wankmüller, R., Denier van der Gon, H., Kuenen, J. J. P.,
936 Klimont, Z., Frost, G., Darras, S., Koffi, B. and Li, M.: HTAP_v2.2: a mosaic of regional and
937 global emission grid maps for 2008 and 2010 to study hemispheric transport of air pollution,
938 *Atmos. Chem. Phys.*, 15(19), 11411–11432, 2015.
- 939 Jathar, S. H., Gordon, T. D., Hennigan, C. J., Pye, H. O. T., Pouliot, G., Adams, P. J., Donahue,
940 N. M. and Robinson, A. L.: Unspeciated organic emissions from combustion sources and their
941 influence on the secondary organic aerosol budget in the United States, *Proc. Natl. Acad. Sci. U.*
942 *S. A.*, 111(29), 10473–10478, 2014.
- 943 Jena, C., Ghude, S. D., Kulkarni, R., Debnath, S., Kumar, R., Soni, V. K., Acharja, P., Kulkarni,
944 S. H., Khare, M., Kaginalkar, A. J., Chate, D. M., Ali, K., Nanjundiah, R. S. and Rajeevan, M.
945 N.: Evaluating the sensitivity of fine particulate matter (PM_{2.5}) simulations to chemical
946 mechanism in Delhi, *Atmos. Chem. Phys. Discuss.*, doi:10.5194/acp-2020-673, 2020.
- 947 Jimenez, J. L., Canagaratna, M. R., Donahue, N. M., Prevot, A. S. H., Zhang, Q., Kroll, J. H.,
948 DeCarlo, P. F., Allan, J. D., Coe, H., Ng, N. L., Aiken, A. C., Docherty, K. S., Ulbrich, I. M.,
949 Grieshop, A. P., Robinson, A. L., Duplissy, J., Smith, J. D., Wilson, K. R., Lanz, V. A., Hueglin,
950 C., Sun, Y. L., Tian, J., Laaksonen, A., Raatikainen, T., Rautiainen, J., Vaattovaara, P., Ehn, M.,
951 Kulmala, M., Tomlinson, J. M., Collins, D. R., Cubison, M. J., Dunlea, E. J., Huffman, J. A.,
952 Onasch, T. B., Alfarra, M. R., Williams, P. I., Bower, K., Kondo, Y., Schneider, J., Drewnick, F.,
953 Borrmann, S., Weimer, S., Demerjian, K., Salcedo, D., Cottrell, L., Griffin, R., Takami, A.,
954 Miyoshi, T., Hatakeyama, S., Shimono, A., Sun, J. Y., Zhang, Y. M., Dzepina, K., Kimmel, J. R.,
955 Sueper, D., Jayne, J. T., Herndon, S. C., Trimborn, A. M., Williams, L. R., Wood, E. C.,
956 Middlebrook, A. M., Kolb, C. E., Baltensperger, U. and Worsnop, D. R.: Evolution of organic
957 aerosols in the atmosphere, *Science*, 326(5959), 1525–1529, 2009.
- 958 Khare, P. and Gentner, D. R.: Considering the future of anthropogenic gas-phase organic
959 compound emissions and the increasing influence of non-combustion sources on urban air
960 quality, *Atmos. Chem. Phys.*, 18(8), 5391–5413, 2018.
- 961 Kleinman, L. I., Daum, P. H., Lee, Y.-N., Senum, G. I., Springston, S. R., Wang, J., Berkowitz,
962 C., Hubbe, J., Zaveri, R. A., Brechtel, F. J., Jayne, J., Onasch, T. B. and Worsnop, D.: Aircraft
963 observations of aerosol composition and ageing in New England and Mid-Atlantic States during
964 the summer 2002 New England Air Quality Study field campaign, *J. Geophys. Res. D: Atmos.*,
965 112(D9), D09310, 2007.
- 966 Kondo, Y., Morino, Y., Fukuda, M., Kanaya, Y., Miyazaki, Y., Takegawa, N., Tanimoto, H.,



- 967 McKenzie, R., Johnston, P., Blake, D. R., Murayama, T. and Koike, M.: Formation and transport
968 of oxidized reactive nitrogen, ozone, and secondary organic aerosol in Tokyo, *J. Geophys. Res.*
969 *D: Atmos.*, 113(D21), D21310, 2008.
- 970 Koo, B., Knipping, E. and Yarwood, G.: 1.5-Dimensional volatility basis set approach for
971 modeling organic aerosol in CAMx and CMAQ, *Atmos. Environ.*, 95, 158–164, 2014.
- 972 Krewski, D., Jerrett, M., Burnett, R. T., Ma, R., Hughes, E., Shi, Y., Turner, M. C., Arden, C.,
973 Thurston, G., Calle, E. E., Thun, M. J., Beckerman, B., Deluca, P., Finkelstein, N., Ito, K.,
974 Moore, D. K., Newbold, K. B., Ramsay, T., Ross, Z., Shin, H. and Tempalski, B.: Extended
975 Follow-Up and Spatial Analysis of the American Cancer Society Study Linking Particulate Air
976 Pollution and Mortality Number 140 May 2009 PRESS VERSION., 2009.
- 977 Kuwata, M., Zorn, S. R. and Martin, S. T.: Using Elemental Ratios to Predict the Density of
978 Organic Material Composed of Carbon, Hydrogen, and Oxygen, *Environ. Sci. Technol.*, 46(2),
979 787–794, 2012.
- 980 Lacey, F. G., Henze, D. K., Lee, C. J., van Donkelaar, A. and Martin, R. V.: Transient climate
981 and ambient health impacts due to national solid fuel cookstove emissions, *Proc. Natl. Acad. Sci.*
982 *U. S. A.*, 114(6), 1269–1274, 2017.
- 983 Landrigan, P. J., Fuller, R., Acosta, N. J. R., Adeyi, O., Arnold, R., Basu, N., Baldé, A. B.,
984 Bertollini, R., Bose-O'Reilly, S., Boufford, J. I., Breyse, P. N., Chiles, T., Mahidol, C.,
985 Coll-Seck, A. M., Cropper, M. L., Fobil, J., Fuster, V., Greenstone, M., Haines, A., Hanrahan, D.,
986 Hunter, D., Khare, M., Krupnick, A., Lanphear, B., Lohani, B., Martin, K., Mathiasen, K. V.,
987 McTeer, M. A., Murray, C. J. L., Ndahimananjara, J. D., Perera, F., Potočnik, J., Preker, A. S.,
988 Ramesh, J., Rockström, J., Salinas, C., Samson, L. D., Sandilya, K., Sly, P. D., Smith, K. R.,
989 Steiner, A., Stewart, R. B., Suk, W. A., van Schayck, O. C. P., Yadama, G. N., Yumkella, K. and
990 Zhong, M.: The Lancet Commission on pollution and health, *Lancet*, 391(10119), 462–512,
991 2018.
- 992 Lelieveld, J., Evans, J. S., Fnais, M., Giannadaki, D. and Pozzer, A.: The contribution of outdoor
993 air pollution sources to premature mortality on a global scale, *Nature*, 525(7569), 367–371, 2015.
- 994 Liao, J., Hanisco, T. F., Wolfe, G. M., St. Clair, J., Jimenez, J. L., Campuzano-Jost, P., Nault, B.,
995 A., Fried, A., Marais, E. A., Gonzalez Abad, G., Chance, K., Jethva, H. T., Ryerson, T. B.,
996 Warneke, C. and Wisthaler, A.: Towards a satellite formaldehyde – in situ hybrid estimate for
997 organic aerosol abundance, *Atmos. Chem. Phys.*, 19(5), 2765–2785, 2019.
- 998 Li, M., Liu, H., Geng, G., Hong, C., Liu, F., Song, Y., Tong, D., Zheng, B., Cui, H., Man, H.,
999 Zhang, Q. and He, K.: Anthropogenic emission inventories in China: a review, *Natl Sci Rev*,
1000 4(6), 834–866, 2017.
- 1001 Li, M., Zhang, Q., Zheng, B., Tong, D., Lei, Y., Liu, F., Chaopeng, H., Kang, S., Yan, L., Zhang,
1002 Y., Bo, Y., Su, H., Cheng, Y. and He, K.: Persistent growth of anthropogenic non-methane
1003 volatile organic compound (NMVOC) emissions in China during 1990-2017: drivers, speciation



- 1004 and ozone formation potential, *Atmos. Chem. Phys.*, 19, 8897–8913, 2019.
- 1005 Liu, F., Zhang, Q., Tong, D., Zheng, B., Li, M., Huo, H. and He, K. B.: High-resolution
1006 inventory of technologies, activities, and emissions of coal-fired power plants in China from
1007 1990 to 2010, *Atmos. Chem. Phys.*, 15(23), 13299–13317, 2015.
- 1008 Lu, Q., Zhao, Y. and Robinson, A. L.: Comprehensive organic emission profiles for gasoline,
1009 diesel, and gas-turbine engines including intermediate and semi-volatile organic compound
1010 emissions, *Atmos. Chem. Phys.*, 18, 17637–17654, 2018.
- 1011 Ma, P. K., Zhao, Y., Robinson, A. L., Worton, D. R., Goldstein, A. H., Ortega, A. M., Jimenez, J.
1012 L., Zotter, P., Prévôt, A. S. H., Szidat, S. and Hayes, P. L.: Evaluating the impact of new
1013 observational constraints on P-S/IVOC emissions, multi-generation oxidation, and chamber wall
1014 losses on SOA modeling for Los Angeles, CA, *Atmos. Chem. Phys.*, 17(15), 9237–9259, 2017.
- 1015 Marais, E. A., Jacob, D. J., Jimenez, J. L., Campuzano-Jost, P., Day, D. A., Hu, W., Krechmer, J.,
1016 Zhu, L., Kim, P. S., Miller, C. C., Fisher, J. A., Travis, K., Yu, K., Hanisco, T. F., Wolfe, G. M.,
1017 Arkinson, H. L., Pye, H. O. T., Froyd, K. D., Liao, J. and McNeill, V. F.: Aqueous-phase
1018 mechanism for secondary organic aerosol formation from isoprene: application to the southeast
1019 United States and co-benefit of SO₂ emission controls, *Atmos. Chem. Phys.*, 16(3), 1603–1618,
1020 2016.
- 1021 McDonald, B. C., de Gouw, J. A., Gilman, J. B., Jathar, S. H., Akherati, A., Cappa, C. D.,
1022 Jimenez, J. L., Lee-Taylor, J., Hayes, P. L., McKeen, S. A., Cui, Y. Y., Kim, S.-W., Gentner, D.
1023 R., Isaacman-VanWertz, G., Goldstein, A. H., Harley, R. A., Frost, G. J., Roberts, J. M., Ryerson,
1024 T. B. and Trainer, M.: Volatile chemical products emerging as largest petrochemical source of
1025 urban organic emissions, *Science*, 359(6377), 760–764, 2018.
- 1026 Miyakawa, T., Takegawa, N. and Kondo, Y.: Photochemical evolution of submicron aerosol
1027 chemical composition in the Tokyo megacity region in summer, *J. Geophys. Res. D: Atmos.*,
1028 113(D14), D14304, 2008.
- 1029 Molina, L. T., Kolb, C. E., de Foy, B., Lamb, B. K., Brune, W. H., Jimenez, J. L.,
1030 Ramos-Villegas, R., Sarmiento, J., Paramo-Figueroa, V. H., Cardenas, B., Gutierrez-Avedoy, V.
1031 and Molina, M. J.: Air quality in North America's most populous city – overview of the
1032 MCMA-2003 campaign, *Atmos. Chem. Phys.*, 7(10), 2447–2473, 2007.
- 1033 Molina, L. T., Madronich, S., Gaffney, J. S., Apel, E., de Foy, B., Fast, J., Ferrare, R., Herndon,
1034 S., Jimenez, J. L., Lamb, B., Osornio-Vargas, A. R., Russell, P., Schauer, J. J., Stevens, P. S.,
1035 Volkamer, R. and Zavala, M.: An overview of the MILAGRO 2006 Campaign: Mexico City
1036 emissions and their transport and transformation, *Atmos. Chem. Phys.*, 10(18), 8697–8760,
1037 2010.
- 1038 Morino, Y., Tanabe, K., Sato, K. and Ohara, T.: Secondary organic aerosol model
1039 intercomparison based on secondary organic aerosol to odd oxygen ratio in Tokyo, *J. Geophys.*
1040 *Res.: Atmos.*, 119(23), 13,489–13,505, 2014.



- 1041 Nault, B. A., Campuzano-Jost, P., Day, D. A., Schroder, J. C., Anderson, B., Beyersdorf, A. J.,
1042 Blake, D. R., Brune, W. H., Choi, Y., Corr, C. A., de Gouw, J. A., Dibb, J., DiGangi, J. P., Diskin,
1043 G. S., Fried, A., Huey, L. G., Kim, M. J., Knote, C. J., Lamb, K. D., Lee, T., Park, T., Pusede, S.
1044 E., Scheuer, E., Thornhill, K. L., Woo, J.-H. and Jimenez, J. L.: Secondary Organic Aerosol
1045 Production from Local Emissions Dominates the Organic Aerosol Budget over Seoul, South
1046 Korea, during KORUS-AQ, *Atmos. Chem. Phys.*, 18, 17769–17800, 2018.
- 1047 Pai, S. J., Heald, C. L., Pierce, J. R., Farina, S. C., Marais, E. A., Jimenez, J. L.,
1048 Campuzano-Jost, P., Nault, B. A., Middlebrook, A. M., Coe, H., Shilling, J. E., Bahreini, R.,
1049 Dingle, J. H. and Vu, K.: An evaluation of global organic aerosol schemes using airborne
1050 observations, *Atmos. Chem. Phys.*, 20(5), 2637–2665, 2020.
- 1051 Pankow, J. F. and Asher, W. E.: SIMPOL.1: a simple group contribution method for predicting
1052 vapor pressures and enthalpies of vaporization of multifunctional organic compounds, *Atmos.*
1053 *Chem. Phys.*, 8(10), 2773–2796, 2008.
- 1054 Park, R. J., Jacob, D. J., Palmer, P. I., Clarke, A. D., Weber, R. J., Zondlo, M. A., Eisele, F. L.,
1055 Bandy, A. R., Thornton, D. C., Sachse, G. W. and Bond, T. C.: Export efficiency of black carbon
1056 aerosol in continental outflow: Global implications, *J. Geophys. Res. D: Atmos.*, 110(D11),
1057 D11205, 2005.
- 1058 Park, R. J., Jacob, D. J., Kumar, N. and Yantosca, R. M.: Regional visibility statistics in the
1059 United States: Natural and transboundary pollution influences, and implications for the Regional
1060 Haze Rule, *Atmos. Environ.*, 40(28), 5405–5423, 2006.
- 1061 Parrish, D. D., Kuster, W. C., Shao, M., Yokouchi, Y., Kondo, Y., Goldan, P. D., de Gouw, J. A.,
1062 Koike, M. and Shirai, T.: Comparison of air pollutant emissions among mega-cities, *Atmos.*
1063 *Environ.*, 43(40), 6435–6441, 2009.
- 1064 Peng, Z. and Jimenez, J. L.: KinSim: A Research-Grade, User-Friendly, Visual Kinetics
1065 Simulator for Chemical-Kinetics and Environmental-Chemistry Teaching, *J. Chem. Educ.*, 96(4),
1066 806–811, 2019.
- 1067 Platt, S. M., Haddad, I. E., Pieber, S. M., Huang, R.-J., Zardini, A. A., Clairotte, M.,
1068 Suarez-Bertoa, R., Barmet, P., Pfaffenberger, L., Wolf, R., Slowik, J. G., Fuller, S. J., Kalberer,
1069 M., Chirico, R., Dommen, J., Astorga, C., Zimmermann, R., Marchand, N., Hellebust, S.,
1070 Temime-Roussel, B., Baltensperger, U. and Prévôt, A. S. H.: Two-stroke scooters are a dominant
1071 source of air pollution in many cities, *Nat. Commun.*, 5(1), 3749, 2014.
- 1072 Pollack, I. B., Ryerson, T. B., Trainer, M., Neuman, J. A., Roberts, J. M. and Parrish, D. D.:
1073 Trends in ozone, its precursors, and related secondary oxidation products in Los Angeles,
1074 California: A synthesis of measurements from 1960 to 2010, *J. Geophys. Res. D: Atmos.*,
1075 118(11), 5893–5911, 2013.
- 1076 Punger, E. M. and West, J. J.: The effect of grid resolution on estimates of the burden of ozone
1077 and fine particulate matter on premature mortality in the USA, *Air Qual. Atmos. Health*, 6(3),



1078 563–573, 2013.

1079 Pye, H. O. T. and Seinfeld, J. H.: A global perspective on aerosol from low-volatility organic
1080 compounds, *Atmos. Chem. Phys.*, 10, 4377–4401, 2010.

1081 Ridley, D. A., Heald, C. L., Ridley, K. J. and Kroll, J. H.: Causes and consequences of
1082 decreasing atmospheric organic aerosol in the United States, *Proc. Natl. Acad. Sci. U. S. A.*,
1083 115(2), 290–295, 2018.

1084 Robinson, A. L., Donahue, N. M., Shrivastava, M. K., Weitkamp, E. A., Sage, A. M., Grieshop,
1085 A. P., Lane, T. E., Pierce, J. R. and Pandis, S. N.: Rethinking Organic Aerosols: Semivolatile
1086 Emissions and Photochemical Aging, *Science*, 315(5816), 1259–1262, 2007.

1087 Rumble, J. R., Ed.: *CRC Handbook of Chemistry and Physics*, 100th Edition, 2019 - 2020,
1088 Taylor & Francis Group., 2019.

1089 Ryerson, T. B., Andrews, A. E., Angevine, W. M., Bates, T. S., Brock, C. A., Cairns, B., Cohen,
1090 R. C., Cooper, O. R., de Gouw, J. A., Fehsenfeld, F. C., Ferrare, R. A., Fischer, M. L., Flagan, R.
1091 C., Goldstein, A. H., Hair, J. W., Hardesty, R. M., Hostetler, C. A., Jimenez, J. L., Langford, A.
1092 O., McCauley, E., McKeen, S. A., Molina, L. T., Nenes, A., Oltmans, S. J., Parrish, D. D.,
1093 Pederson, J. R., Pierce, R. B., Prather, K., Quinn, P. K., Seinfeld, J. H., Senff, C. J., Sorooshian,
1094 A., Stutz, J., Surratt, J. D., Trainer, M., Volkamer, R., Williams, E. J. and Wofsy, S. C.: The 2010
1095 California Research at the Nexus of Air Quality and Climate Change (CalNex) field study, *J.*
1096 *Geophys. Res. D: Atmos.*, 118(11), 5830–5866, 2013.

1097 Sacks, J., Buckley, B., Alexis, N., Angrish, M., Beardslee, R., Benson, A., Brown, J., Buckley,
1098 B., Campen, M., Chan, E., Coffman, E., Davis, A., Dutton, S. J., Eftim, S., Gandy, J., Hemming,
1099 B. L., Hines, E., Holliday, K., Kerminen, V.-M., Kiomourtzoglou, M.-A., Kirrane, E., Kotchmar,
1100 D., Koturbash, I., Kulmala, M., Lassiter, M., Limaye, V., Ljungman, P., Long, T., Luben, T.,
1101 Malm, W., McDonald, J. F., McDow, S., Mickley, L., Mikati, I., Mulholland, J., Nichols, J.,
1102 Patel, M. M., Pinder, R., Pinto, J. P., Rappazzo, K., Richmond-Bryant, J., Rosa, M., Russell, A.,
1103 Schichtel, B., Stewart, M., Stanek, L. W., Turner, M., Van Winkle, L., Wagner, J., Weaver,
1104 Christopher, Wellenius, G., Whitsel, E., Yeckel, C., Zanutti, A. and Zhang, M.: Integrated
1105 Science Assessment (ISA) for Particulate Matter (Final Report, Dec 2019), Environmental
1106 Protection Agency. [online] Available from:
1107 <https://cfpub.epa.gov/ncea/isa/recordisplay.cfm?deid=347534> (Accessed 20 October 2020),
1108 2019.

1109 Schroder, J. C., Campuzano-Jost, P., Day, D. A., Shah, V., Larson, K., Sommers, J. M., Sullivan,
1110 A. P., Campos, T., Reeves, J. M., Hills, A., Hornbrook, R. S., Blake, N. J., Scheuer, E., Guo, H.,
1111 Fibiger, D. L., McDuffie, E. E., Hayes, P. L., Weber, R. J., Dibb, J. E., Apel, E. C., Jaeglé, L.,
1112 Brown, S. S., Thornton, J. A. and Jimenez, J. L.: Sources and Secondary Production of Organic
1113 Aerosols in the Northeastern US during WINTER, *J. Geophys. Res. D: Atmos.*,
1114 doi:10.1029/2018JD028475, 2018.

1115 Seinfeld, J. H. and Pandis, S. N.: *Atmospheric Chemistry and Physics: From Air Pollution to*



- 1116 Climate Change, Second., John Wiley & Sons, Inc., Hoboken, NJ USA., 2006.
- 1117 Shaddick, G., Thomas, M. L., Amini, H., Broday, D., Cohen, A., Frostad, J., Green, A., Gumy,
1118 S., Liu, Y., Martin, R. V., Pruss-Ustun, A., Simpson, D., van Donkelaar, A. and Brauer, M.: Data
1119 Integration for the Assessment of Population Exposure to Ambient Air Pollution for Global
1120 Burden of Disease Assessment, *Environ. Sci. Technol.*, 52(16), 9069–9078, 2018.
- 1121 Shah, V., Jaeglé, L., Thornton, J. A., Lopez-Hilfiker, F. D., Lee, B. H., Schroder, J. C.,
1122 Campuzano-Jost, P., Jimenez, J. L., Guo, H., Sullivan, A. P., Weber, R. J., Green, J. R., Fiddler,
1123 M. N., Bililign, S., Campos, T. L., Stell, M., Weinheimer, A. J., Montzka, D. D. and Brown, S.
1124 S.: Chemical feedbacks weaken the wintertime response of particulate sulfate and nitrate to
1125 emissions reductions over the eastern United States, *Proc. Natl. Acad. Sci. U. S. A.*, 115(32),
1126 8110–8115, 2018.
- 1127 Shah, V., Jaeglé, L., Jimenez, J. L., Schroder, J. C., Campuzano-Jost, P., Campos, T. L., Reeves,
1128 J. M., Stell, M., Brown, S. S., Lee, B. H., Lopez-Hilfiker, F. D. and Thornton, J. A.: Widespread
1129 Pollution from Secondary Sources of Organic Aerosols during Winter in the Northeastern United
1130 States, *Geophys. Res. Lett.*, doi:10.1029/2018GL081530, 2019.
- 1131 Shrivastava, M., Cappa, C. D., Fan, J., Goldstein, A. H., Guenther, A. B., Jimenez, J. L., Kuang,
1132 C., Laskin, A., Martin, S. T., Ng, N. L., Petaja, T., Pierce, J. R., Rasch, P. J., Roldin, P., Seinfeld,
1133 J. H., Shilling, J., Smith, J. N., Thornton, J. A., Volkamer, R., Wang, J., Worsnop, D. R., Zaveri,
1134 R. A., Zelenyuk, A. and Zhang, Q.: Recent advances in understanding secondary organic aerosol:
1135 Implications for global climate forcing, *Rev. Geophys.*, 55(2), 509–559, 2017.
- 1136 Silva, R. A., Adelman, Z., Fry, M. M. and West, J. J.: The Impact of Individual Anthropogenic
1137 Emissions Sectors on the Global Burden of Human Mortality due to Ambient Air Pollution,
1138 *Environ. Health Perspect.*, 124(11), 1776–1784, 2016.
- 1139 Singh, A., Satish, R. V. and Rastogi, N.: Characteristics and sources of fine organic aerosol over
1140 a big semi-arid urban city of western India using HR-ToF-AMS, *Atmos. Environ.*, 208, 103–112,
1141 2019.
- 1142 Stewart, G. J., Nelson, B. S., Acton, W. J. F., Vaughan, A. R., Farren, N. J., Hopkins, J. R., Ward,
1143 M. W., Swift, S. J., Arya, R., Mondal, A., Jangirh, R., Ahlawat, S., Yadav, L., Sharma, S. K.,
1144 Yunus, S. S. M., Hewitt, C. N., Nemitz, E., Mullinger, N., Gadi, R., Sahu, L. K., Tripathi, N.,
1145 Rickard, A. R., Lee, J. D., Mandal, T. K. and Hamilton, J. F.: Emissions of intermediate-volatility
1146 and semi-volatile organic compounds from domestic fuels used in Delhi, India, *Atmos. Chem.*
1147 *Phys. Discuss.*, doi:10.5194/acp-2020-860, 2020.
- 1148 The International GEOS-Chem User Community: geoschem/geos-chem: GEOS-Chem 12.0.0
1149 release, , doi:10.5281/ZENODO.1343547, 2018.
- 1150 Toon, O. B., Maring, H., Dibb, J., Ferrare, R., Jacob, D. J., Jensen, E. J., Luo, Z. J., Mace, G. G.,
1151 Pan, L. L., Pfister, L., Rosenlof, K. H., Redemann, J., Reid, J. S., Singh, H. B., Thompson, A.
1152 M., Yokelson, R., Minnis, P., Chen, G., Jucks, K. W. and Pszenny, A.: Planning, implementation,



- 1153 and scientific goals of the Studies of Emissions and Atmospheric Composition, Clouds and
1154 Climate Coupling by Regional Surveys (SEAC⁴RS) field mission, *J. Geophys. Res. D: Atmos.*,
1155 121(9), 4967–5009, 2016.
- 1156 Tsimpidi, A. P., Karydis, V. A., Zavala, M., Lei, W., Molina, L., Ulbrich, I. M., Jimenez, J. L. and
1157 Pandis, S. N.: Evaluation of the volatility basis-set approach for the simulation of organic aerosol
1158 formation in the Mexico City metropolitan area, *Atmos. Chem. Phys.*, 10(2), 525–546, 2010.
- 1159 Vaden, T. D., Imre, D., Beránek, J., Shrivastava, M. and Zelenyuk, A.: Evaporation kinetics and
1160 phase of laboratory and ambient secondary organic aerosol, *Proc. Natl. Acad. Sci. U. S. A.*,
1161 108(6), 2190–2195, 2011.
- 1162 Wang, L., Slowik, J. G., Tripathi, N., Bhattu, D., Rai, P., Kumar, V., Vats, P., Satish, R.,
1163 Baltensperger, U., Ganguly, D., Rastogi, N., Sahu, L. K., Tripathi, S. N. and Prévôt, A. S. H.:
1164 Source characterization of volatile organic compounds measured by proton-transfer-reaction
1165 time-of-flight mass spectrometers in Delhi, India, *Atmos. Chem. Phys.*, 20(16), 9753–9770,
1166 2020.
- 1167 Wang, M., Shao, M., Chen, W., Yuan, B., Lu, S., Zhang, Q., Zeng, L. and Wang, Q.: A
1168 temporally and spatially resolved validation of emission inventories by measurements of ambient
1169 volatile organic compounds in Beijing, China, *Atmos. Chem. Phys.*, 14(12), 5871–5891, 2014.
- 1170 Wang, Y. Q., Zhang, X. Y., Sun, J. Y., Zhang, X. C., Che, H. Z. and Li, Y.: Spatial and temporal
1171 variations of the concentrations of PM₁₀, PM_{2.5} and PM₁ in China, *Atmos. Chem. Phys.*, 15,
1172 13585–13598, 2015.
- 1173 Warneke, C., McKeen, S. A., de Gouw, J. A., Goldan, P. D., Kuster, W. C., Holloway, J. S.,
1174 Williams, E. J., Lerner, B. M., Parrish, D. D., Trainer, M., Fehsenfeld, F. C., Kato, S., Atlas, E.
1175 L., Baker, A. and Blake, D. R.: Determination of urban volatile organic compound emission
1176 ratios and comparison with an emissions database, *J. Geophys. Res. D: Atmos.*, 112(D10),
1177 doi:10.1029/2006JD007930, 2007.
- 1178 Warneke, C., de Gouw, J. A., Holloway, J. S., Peischl, J., Ryerson, T. B., Atlas, E., Blake, D.,
1179 Trainer, M. and Parrish, D. D.: Multiyear trends in volatile organic compounds in Los Angeles,
1180 California: Five decades of decreasing emissions, *J. Geophys. Res. D: Atmos.*, 117(D21),
1181 D00V17, 2012.
- 1182 Wood, E. C., Canagaratna, M. R., Herndon, S. C., Onasch, T. B., Kolb, C. E., Worsnop, D. R.,
1183 Kroll, J. H., Knighton, W. B., Seila, R., Zavala, M., Molina, L. T., Decarlo, P. F., Jimenez, J. L.,
1184 Weinheimer, A. J., Knapp, D. J., Jobson, B. T., Stutz, J., Kuster, W. C. and Williams, E. J.:
1185 Investigation of the correlation between odd oxygen and secondary organic aerosol in Mexico
1186 City and Houston, *Atmos. Chem. Phys.*, 10(18), 8947–8968, 2010.
- 1187 Worton, D. R., Isaacman, G., Gentner, D. R., Dallmann, T. R., Chan, A. W. H., Ruehl, C.,
1188 Kirchstetter, T. W., Wilson, K. R., Harley, R. A. and Goldstein, A. H.: Lubricating Oil Dominates
1189 Primary Organic Aerosol Emissions from Motor Vehicles, *Environ. Sci. Technol.*, 48(7),



1190 3698–3706, 2014.

1191 Zhang, Q., Alfarra, M. R., Worsnop, D. R., James, D., Coe, H., Canagaratna, M. R. and Jimenez,
1192 J. L.: Deconvolution and Quantification of Hydrocarbon-like and Oxygenated Organic Aerosols
1193 Based on Aerosol Mass Spectrometry Deconvolution and Quantification of Hydrocarbon-like
1194 and Oxygenated Organic Aerosols Based on Aerosol Mass Spectrometry, *Environ. Sci. Technol.*,
1195 39(13), 4938–4952, 2005.

1196 Zhang, Q., Streets, D. G., Carmichael, G. R., He, K. B., Huo, H., Kannari, A., Klimont, Z., Park,
1197 I. S., Reddy, S., Fu, J. S., Chen, D., Duan, L., Lei, Y., Wang, L. T. and Yao, Z. L.: Asian
1198 emissions in 2006 for the NASA INTEX-B mission, *Atmos. Chem. Phys.*, 9(14), 5131–5153,
1199 2009.

1200 Zhang, Q. J., Beekmann, M., Freney, E., Sellegri, K., Pichon, J. M., Schwarzenboeck, A.,
1201 Colomb, A., Bourriane, T., Michoud, V. and Borbon, A.: Formation of secondary organic
1202 aerosol in the Paris pollution plume and its impact on surrounding regions, *Atmos. Chem. Phys.*,
1203 15(24), 13973–13992, 2015.

1204 Zhao, Y., Hennigan, C. J., May, A. A., Daniel, S., Gouw, J. A. D., Gilman, J. B., Kuster, W. C.
1205 and Robinson, A. L.: Intermediate-Volatility Organic Compounds: A Large Source of Secondary
1206 Organic Aerosol, *Environ. Sci. Technol.*, 48(23), 13743–13750, 2014.

1207 Zhao, Y., Saleh, R., Saliba, G., Presto, A. A., Gordon, T. D., Drozd, G. T., Goldstein, A. H.,
1208 Donahue, N. M. and Robinson, A. L.: Reducing secondary organic aerosol formation from
1209 gasoline vehicle exhaust, *Proc. Natl. Acad. Sci. U. S. A.*, 114(27), 6984–6989, 2017.

1210 Zheng, B., Huo, H., Zhang, Q., Yao, Z. L., Wang, X. T., Yang, X. F., Liu, H. and He, K. B.:
1211 High-resolution mapping of vehicle emissions in China in 2008, *Atmos. Chem. Phys.*, 14(18),
1212 9787–9805, 2014.

1213 Zheng, B., Tong, D., Li, M., Liu, F., Hong, C., Geng, G., Li, H., Li, X., Peng, L., Qi, J., Yan, L.,
1214 Zhang, Y., Zhao, H., Zheng, Y., He, K. and Zhang, Q.: Trends in China's anthropogenic
1215 emissions since 2010 as the consequence of clean air actions, *Atmos. Chem. Phys.*, 18(19),
1216 14095–14111, 2018.

1217